Original

Meng, Q.; Zhang, W.; Zhou, F.; Liao, Y.; Yu, P.; Tang, Y.; Ma, X.; Di, T.; Ding, R.; Ni, X.; Zeng, D.; Schrum, C.:

Water Oxygen Consumption Rather Than Sediment Oxygen Consumption Drives the Variation of Hypoxia on the East China Sea Shelf.

In: Journal of Geophysical Research : Biogeosciences. Vol. 127 (2022) 2, e2021JG006705.

First published online by AGU: 26.01.2022

https://dx.doi.org/10.1029/2021JG006705

JGR Biogeosciences

RESEARCH ARTICLE
10.1029/2021JG006705

Key Points:

- Contributions of porewater advection, molecular diffusion and bioturbation to sediment oxygen consumption in East China Sea are quantified
- Water oxygen consumption is the major driver of the variation of hypoxia rather than sediment oxygen consumption
- Mild hydrodynamics increase water oxygen consumption but weaken sediment oxygen consumption by suppressing porewater advection

Supporting Information:

Supporting Information may be found in the online version of this article.

Correspondence to:

Q. Meng and F. Zhou,
q.meng@sio.org.cn;
zhoufeng@sio.org.cn

Citation:

Meng, Q., Zhang, W., Zhou, F., Liao, Y., Yu, P., Tang, Y., et al. (2022). Water oxygen consumption rather than sediment oxygen consumption drives the variation of hypoxia on the East China Sea shelf. *Journal of Geophysical Research: Biogeosciences*, *127*, e2021JG006705. https://doi.org/10.1029/2021JG006705

Received 5 NOV 2021
Accepted 17 JAN 2022

Water Oxygen Consumption Rather Than Sediment Oxygen Consumption Drives the Variation of Hypoxia on the East China Sea Shelf

Qicheng Meng[1,2,3], Wenyan Zhang[4], Feng Zhou[1,2,5], Yibo Liao[1,2,6], Peisong Yu[6], Yanbin Tang[2,6], Xiao Ma[1,2], Di Tian[1,2], Ruibin Ding[7,8], Xiaobo Ni[1,2], Dingyong Zeng[1,2], and Corinna Schrum[4]

[1]State Key Laboratory of Satellite Ocean Environment Dynamics, Second Institute of Oceanography, Ministry of Natural Resources, Hangzhou, China, [2]Observation and Research Station of Yangtze River Delta Marine Ecosystems, Ministry of Natural Resources, Zhoushan, China, [3]Key Laboratory of Ocean Space Resource Management Technology, Ministry of Natural Resources, Marine Academy of Zhejiang Province, Hangzhou, China, [4]Institute of Coastal Systems – Analysis and Modeling, Helmholtz–Zentrum Hereon, Geesthacht, Germany, [5]School of Oceanography, Shanghai Jiao Tong University, Shanghai, China, [6]Key Laboratory of Marine Ecosystem Dynamics, Second Institute of Oceanography, Ministry of Natural Resources, Hangzhou, China, [7]Institute of Polar and Ocean Technology, Second Institute of Oceanography, Ministry of Natural Resources, Hangzhou, China, [8]Indian Ocean Center, Second Institute of Oceanography, Ministry of Natural Resources, Hangzhou, China

Abstract Sediment oxygen consumption (SOC) is important in modulating the oxygen budget in the East China Sea where seasonal hypoxia occurs. Porewater advection, molecular diffusion and bioturbation supply oxygen for sedimentary organic matter degradation. A pelagic-benthic coupled model was applied to quantify the SOC. A comparison with observations showed good model performance in reproducing the hydrographic and ecological environments, particularly for the interannual variation in the hypoxic zone. Simulation results show that porewater-advection-induced flux is the predominant component of the SOC in sandy areas on the Changjiang bank and outer shelves, while the bioturbation-induced flux is predominant at mud depocenters. By comparing SOC to the water oxygen consumption (WOC) below the pycnocline, the contribution of SOC is generally below ~40% in the hypoxic zone. The spatial distribution of SOC in summer is relatively steady from year to year, while the high WOC patches explain more about the interannual variation in the hypoxic zone. WOC rather than SOC drives the variation of hypoxia. Particularly on the Changjiang bank, milder hydrodynamics are favorable for both the higher WOC and bioturbation-induced benthic oxygen flux but substantially suppress the porewater advective flux, which results in the net lower contribution of SOC to hypoxia. This finding may shed light on other pelagic-benthic coupling processes in coastal shelf seas where hypoxia occurs on permeable sediments.

Plain Language Summary Oxygen exhaustion or hypoxia issues have been increasingly found in coastal waters. The seasonal hypoxic zone off the Changjiang Estuary in the East China Sea is one of the largest coastal hypoxic zones worldwide. It is of significance to understand the underlying drivers of its formation as well as its variation. The oxygen extracted from the water-sediment interface has been realized to be an important de-oxygenation way. Porewater flow, molecular diffusion and macrobenthos reworking facilitate sediment oxygen consumption in deeper layers. We used a model to simulate the three-dimensional sediment interacting with the water column. We found that although the sediment oxygen consumption showed great spatial heterogeneity and complex temporal variations, its pattern did not change much in each summer relative to the highly variable hypoxic zone. Sediment oxygen consumption is not the major driver of the variation of hypoxia. Nevertheless, it has complex variations coupled with the pelagic system in association with hypoxia. Additionally, the buffering effect of the benthic system suggests the challenge of mitigating hypoxia effectively by reducing marine primary production.

1. Introduction

Dissolved oxygen (DO) is essential for most marine creatures. A hypoxic threshold, usually defined as DO being approximately 2–3 mg/L, leads to an abrupt constraint on aerobic biogeochemical processes and long-term stress on the marine ecosystem in terms of biogeochemical cycles, biodiversity and resilience (Fennel & Testa, 2019;

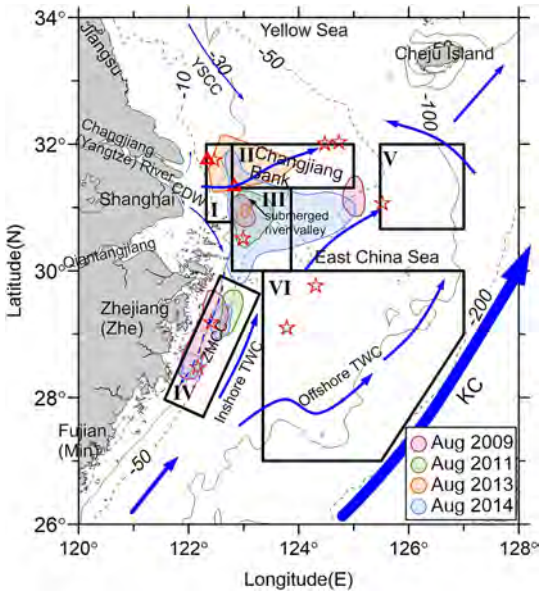

Figure 1. The geographic location of the ECS with bathymetry and major components of circulation. TWC, ZMCC, CDW, YSCC and KC are the Taiwan Warm Current, Zhe-Min Coastal Current, Changjiang diluted water, Yellow Sea Coastal Current, and Kuroshio Current, respectively. Six study regions, that is, Regions I to VI, are specified by black polygons. The hypoxic zones (DO ≤ 3 mg/L) found by cruises in August of 2009, 2011, 2013 and 2014 are outlined with different colors. Sampling stations for SOC from Cai et al. (2014) and Song et al. (2016) are labeled by red triangles and red pentagrams, respectively.

Vaquer-Sunyer & Duarte, 2008; Wu, 2002). Both direct anthropogenic discharge and climate change contribute to aggravating hypoxia issues, especially in coastal waters (Breitburg et al., 2018; Diaz & Rosenberg, 2008; Fennel & Testa, 2019; Rabalais et al., 2010; K. Wang et al., 2021). A mechanistic understanding of coastal hypoxia issues is crucial for the reliable forecasting of hypoxia events (Fennel et al., 2019; Testa et al., 2017; W. Zhang et al., 2018; F. Zhou et al., 2017) and for making efficient and effective terrestrial pollutant discharge control policies to mitigate hypoxia and restore productive marine ecosystems (Conley et al., 2009; Fennel & Laurent, 2018; Große et al., 2019; F. Zhou et al., 2020).

Oxygen is consumed by the degradation of organic matter during its transport in water as well as after deposition on the seabed. Both water oxygen consumption (WOC) and sediment oxygen consumption (SOC) play important roles in the development and deterioration of hypoxia in bottom waters (Fennel et al., 2013; H. Zhang et al., 2017; F. Zhou et al., 2017). The seasonal hypoxic zone off the Changjiang Estuary (CE) in the East China Sea (ECS) is one of the largest coastal hypoxic zones in the world but is less understood than other areas, such as Baltic Sea, Chesapeake Bay, and the northern Gulf of Mexico (C.-C. Chen et al., 2007; Fennel & Testa, 2019; Li et al., 2002; Rabouille et al., 2008; H. Wei et al., 2007). Hypoxia off the CE normally occurs in late spring to early autumn and prevails in summer (Chi et al., 2020; B. Wang et al., 2012). A ground challenge is to understand the drivers causing the formation of hypoxia off the CE as well as its remarkable interannual variation (Figure 1) (F. Zhou et al., 2010, 2020; Zhu et al., 2011). There have been an increasing number of studies on physical and biogeochemical processes within the pelagic system. Firstly, stratification is a pre-condition for the formation and maintenance of hypoxia (Liblik et al., 2020; W. Zhang, Wirtz, et al., 2019; W. Zhang, Wu, et al., 2019; F. Zhou et al., 2010). Stratification may be interrupted by episodic strong wind events, for example, typhoons (Ni et al., 2016). Secondly, the excessive organic matter that fuels oxygen depletion mainly comes from oceanic algal blooms (K. Wang et al., 2014; H. Wang et al., 2016). High-biomass diatom blooms are believed to have a causal linkage to hypoxia (B. Wang et al., 2017). However, the locations of diatom blooms and hypoxia do not exactly overlap due to the vertical current shear and time-lag correlation (F. Zhou et al., 2020). Two known drivers of the variation in the hypoxic zone are the dynamically varying Changjiang diluted water (CDW) plume (Y. Wang et al., 2019; W. Zhang, Wu, et al., 2019; F. Zhou et al., 2020) and the non-uniform subsurface offshore advection (F. Zhou et al., 2020). Various observational studies have revealed a significant impact of SOC on the pelagic DO budget in the ECS, despite its spatial and temporal heterogeneity. The conventional ex situ sediment core incubation method, which measures the remineralization rate but overlooks in situ physical disturbances (porewater advection), has been applied by Song et al. (2016), H. Zhang et al. (2017), Zhao et al. (2018) and Chi et al. (2021) in the ECS. Based on sampling at 13 sites in the ECS, Song et al. (2016) deduced that the contribution of SOC to the total local oxygen consumption, which is defined as WOC + SOC, was approximately 20%. In addition, Song et al. (2016) mentioned that most of their sampling sites were dominated by clay or silt, where diffusion is the main driving force for oxygen input to sediment, and only one core incubation from sandy sediment would have underestimated SOC without taking into account porewater advection. H. Zhang et al. (2017) proposed that the contribution of SOC in summer ranged between 80% and 179% based on their estimations of non-overlapping sampling sites. Zhao et al. (2018) estimated that the ratio (SOC to the sum of SOC and WOC) at the Zhe-Min coastal mud belt (ZMCMB) was approximately 18%. Chi et al. (2021) estimated that the contributions of SOC at three stations within the hypoxic zones in summer were 54%, 48% and 44%, respectively. By using $^{224}Ra/^{228}Th$ disequilibrium in the sediment, Cai et al. (2014) found that the contribution of SOC ranged from 6% to 38%. Through analyzing the isotopic fractionation of DO, J. Zhou et al. (2021) found that beneath the pycnocline, the contribution of SOC to the total local oxygen consumption in near-bottom waters varied between 31% and 76%, and in the hypoxic environment, up to 70% of the apparent oxygen utilization was contributed

Table 1
Characteristics in the Studied Regions

Region	Hydrodynamics	Sediment type	Hypoxia	Pelagic-benthic interactions
I	CDW	Muddy	Yes	High primary production, mud depocenter
II	CDW	Sandy	Yes	High primary production, strong tide
III	CDW, TWC	Mixed	Yes	High primary production, shelf valley, advection
IV	ZMCC, TWC	Muddy	Yes	High primary production, mud depocenter, advection
V	CDW, TWC, YSCC, KC	Muddy	No	Low primary production, mud depocenter, advection
VI	TWC	Sandy	No	Low primary production, broad shelf, advection

by WOC. The above-mentioned variability among observations reveals strong heterogeneity of the SOC (Chi et al., 2021).

Numerical models for coastal hypoxia need to incorporate SOC to improve the accuracy. Various models of SOC have been developed in recent years. SOC models are normally coupled with nutrient-phytoplankton-zooplankton-detritus (NPZD)-type pelagic models to resolve biogeochemical processes occurring at the sediment-water interface (Fennel et al., 2006; Laurent et al., 2017). For model application to the ECS, F. Zhou et al. (2017) conducted numerical experiments on the impact of SOC on hypoxia off the CE by coupling the "instantaneous remineralization" SOC module (Fennel et al., 2006) with the Carbon, Silicate and Nitrogen Ecosystem (CoSiNE) model (Chai et al., 2002; Xiu & Chai, 2014). By adding the SOC, the simulated maximum hypoxic zone approximately doubled compared to the simulation results without SOC but had similar distribution patterns. H. Zhang, Fennel, et al. (2020) applied another NPZD-type model with the same SOC module to simulate hypoxia off the CE, suggesting that the impact of SOC could be comparable to or even exceed the WOC beneath the pycnocline in the hypoxic zone. Different from the abovementioned SOC model, W. Zhang et al. (2018) directly appended a sink term of oxygen at the sediment-water interface dependent on bottom temperature and DO concentration, which was proposed by Hetland and DiMarco (2008), to their NPZD-type pelagic model. Their results also suggested a comparable importance of SOC with respect to WOC to the hypoxia off the CE. However, it is worth noting that all SOC models that have been applied to the ECS are based on empirical formulations and do not directly resolve detailed physical and biogeochemical processes affecting vertical oxygen transport and consumption within sediment. In particular, the dynamics of porewater advection affected by bedform migration and the impact of bioturbation, which were both proven to be crucial in mediating oxygen transport and consumption in sandy and muddy sediment, respectively (W. Zhang et al., 2021), are missing in the applied SOC models.

This study aims to further understand the temporal variation and spatial distribution of SOC in the ECS and its contribution to the formation of hypoxia in the summer season. By applying the state-of-the-art benthic-pelagic coupled models introduced in Section 2, the SOC driven by physical, biological and biogeochemical processes was quantified. Simulation results were assessed by comparisons with measured values in Section 3 and analyzed to derive a process-based understanding of SOC dynamics in the study area. Broader implications of our results as well as their uncertainties and limitations are discussed in Section 4, and the main outcomes are concluded in Section 5.

2. Materials and Methods

2.1. Partitioning of the Study Area for Specific Research Interests

To better understand the spatial variation in hypoxia, six regions, as shown in Figure 1, were selected for area-mean analyses, taking into account their distinct features in hydrodynamic conditions, sediment types and pelagic-benthic interactions (Table 1). Region I partially covers the mud depocenter at the Changjiang Subaqueous Delta (CSD; Jia et al., 2018) to the southeast of the CE (Figures 2a and 2b). Its hydrographic environment is predominantly influenced by the CDW in all seasons. Hypoxia occasionally expands to this region (see the hypoxic zones in Figure 1). Region II partially covers a modern tidal sand sheet (TSS) exposed to strong tidal-induced mixing on the Changjiang bank (Figure 2a; Liu, 1997; Xuan et al., 2016). Its hydrographic environment in summer is strongly influenced by the river plume. Hypoxia also occasionally expands to this region (Figure 1). Region III is located at the submerged river valley. Its hydrographic environment is influenced by both the CDW

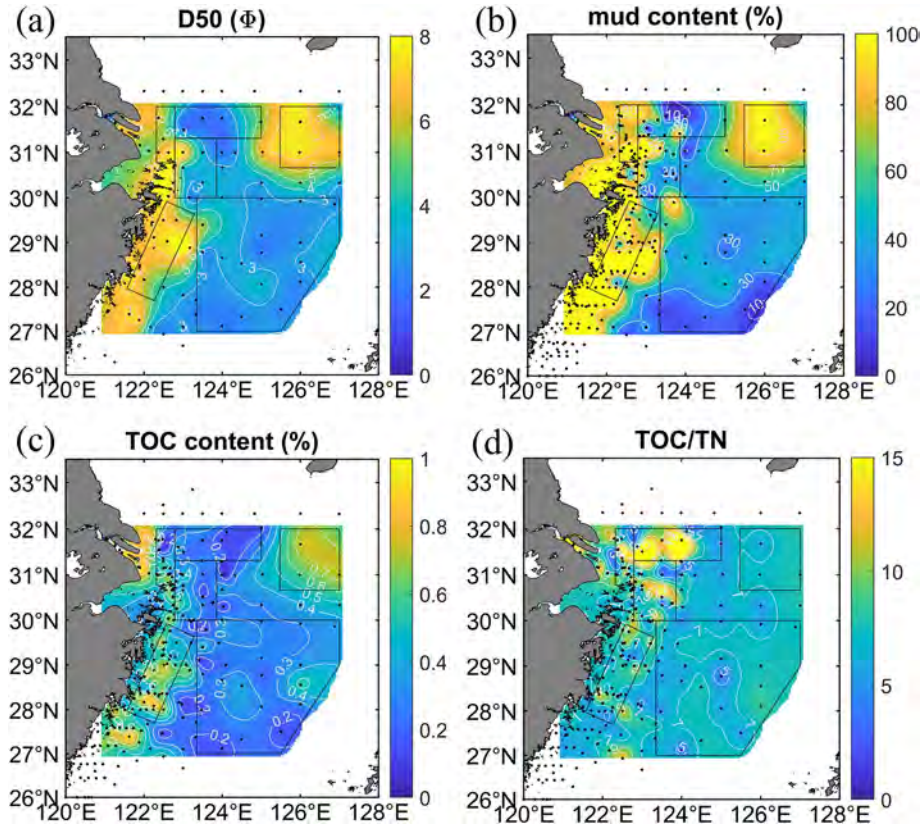

Figure 2. The survey data for median grain size (D50; a), mud content (b), Total organic carbon (TOC) content (c) and the ratio between TOC and total nitrogen (TN; d) in surface sediment from P. Yu et al. (2011) and C. Wang et al. (2020). Black dots indicate the sampling stations. Six study regions are specified by black polygons.

and the TWC. The sediment type is heterogeneous in this region (Figures 2a and 2b). This region represents the core zone of hypoxia that persistently occurs in every observed year (Figure 1). Region IV partially covers the ZMCMB on the inner shelf off the Zhejiang and Fujian provincial coasts. Its hydrographic environment is dominated by the ZMCC with a persistent Zhe-Min coastal front (Figures 2a and 2b). It is also vulnerable to the hypoxia (Figure 1). Region V partially covers the southwestern Cheju Island mud (SWCIM) depocenter (Figures 2a and 2b). The CDW is predominant for the dispersal of fine grains and terrestrial organic carbon (OC) at the modern SWCIM via two pathways: one northeastward branch encountering the southward YSCC and another southward branch entrained by the northward TWC (W. Zhang et al., 2015). Hypoxia was not observed in that region (Figure 1), although the total organic carbon (TOC) content was high in the sediment there (Figure 2c). Extending from the middle shelf to the outer shelf, Region VI partially covers the relict sand area (RSA; Figures 2a and 2b). Its hydrographic environment is predominantly controlled by the TWC. Hypoxia was not occasionally observed there in summer (Figure 1). A higher TOC to total nitrogren (TN) ratio in Regions I, II and III suggests a likely less labile sedimentary TOC in these regions than in other regions (Figure 2d). These six regions are characterized by distinct hydrodynamics, sediment properties and ecological dynamics (Table 1). The pelagic-benthic coupled study can shed light upon the drivers of hypoxia.

2.2. Observational Data

Various observational datasets obtained via remote sensing, in situ ship-borne surveys and ex situ lab analysis were used to initialize or validate the model. A summary of the datasets is given in Table 2.

Data on the spatial distribution of median sediment grain size, grain size compositions, TOC and TN in sediment were mainly derived from the cruise in November 2007 (P. Yu et al., 2011), during which 78 surface (0–5 cm) sediment samples (Table 2) on the ECS shelf were collected and analyzed. The sampling locations can be found

Table 2
Summary of Observational Data Used in the Study

Data type	Usage	Method	Sampling time	No. of stations/ samples	Source
Sea surface temperature (SST)	Validation	Remote sensing	2009–2014	–	NOAA OI SST V2 (Reynolds et al., 2007)
Chlorophyll-a (Chl-a)	Validation	Remote sensing	2009–2014	–	Hao et al. (2019)
Bottom temperature, bottom salinity, bottom DO	Validation	Repetitive ship-borne surveys at the zonal 31°N transect	June, 2009 August, 2009 May, 2011 August, 2011 May, 2012 May, 2013 August, 2013 October, 2013 August, 2014	9 9 6 7 4 7 7 7 9	This study
Hypoxic zones (≤3 mg/L)	Validation	Ship-borne survey	August, 2009 August, 2011 August, 2013 August, 2014	26 26 36 38	F. Zhou et al. (2020)
Median grain size, grain size composition, total organic carbon (TOC) & total nitrogen (TN)	Initial conditions	Lab analyze	November, 2007	78	P. Yu et al. (2011)
Grain size composition, TOC & TN	Initial conditions	Lab analyze	2006–2007	131	Hu et al. (2012); C. Wang et al. (2020)
Benthos	Validation	Lab analyze	July, 2011	12	This study
SOC	Validation	Incubation	June, 2010 October, 2010 May, 2011	3 4 5	Song et al. (2016)
SOC	Validation	224Ra: 228Th disequilibrium	August 2011	2	Cai et al. (2014)

in Figure 2a superimposed by the median grain size, D50. In addition, C. Wang et al. (2020) collected another dataset for grain size compositions and TOC and TN contents on the inner shelf in 2006. We found that the two datasets were consistent. Therefore, these two datasets were merged to increase the spatial resolution (Figures 2b–2d). The mud content, as a sum of silt and clay contents, is interpolated from the data at the sampling stations shown in Figure 2b.

Macrobenthos data collected by a cruise in the ECS were used to assess model performance. A total of 12 stations were sampled during July 2011 (Table 2). Duplicate samples (pooled as one sample) were collected at each site with a grab sampler (0.1 m^3). The samples were sieved with a 0.5-mm mesh sieve and preserved with 5% buffered formalin. In the laboratory, the macrobenthos were sorted and identified to the lowest possible taxonomic level (generally species) and enumerated. The biomass was measured in ash-free dry weight.

To assess the modeled SOC, we collected field measurements from the existing literature. Due to an insufficient spatial resolution, small islands and their adjacent areas were not well presented in the present model. Therefore, field measurements that were close to the shore or small islands were excluded from the model assessment. 12 measurements at 9 sampling stations (Figure 1) on the ECS shelf (Table 2) were collected from Song et al. (2016). Measurements by the batch incubation technique were conducted during three cruises in June 2010, October 2010 and May 2011 (Song et al., 2016). Two measurements at different stations (Figure 1) on the ECS shelf in August 2011 derived by $^{224}Ra/^{228}Th$ disequilibrium in the sediment (Table 2) were collected from Cai et al. (2014).

The hypoxic zones shown in Figure 1 were extracted from four ship-borne surveys presented by F. Zhou et al. (2020) to assess the performance of the pelagic model. The DO at the bottom layer was measured by a sensor mounted on the conductivity, temperature, and depth (CTD) sampling rosette.

The observation and research station of Yangtze River Delta Marine Ecosystems operated by the Ministry of Natural Resources provided repetitively measured temperature, salinity and oxygen data along a zonal transect at latitude 31°N (Table 2) from nearshore to offshore up to 550 km from the coast. This study utilized the measurements at the bottom layer from 2009 to 2014 to assess the model results.

2.3. Numerical Models

2.3.1. Pelagic Model

Pelagic ecosystem dynamics were simulated by a coupled physical-biogeochemical model. The physical module was based on a customized Regional Ocean Modeling Systems (ROMS) model particularly tuned for the ECS (Haidvogel et al., 2008; Shchepetkin & McWilliams, 2005; F. Zhou et al., 2015, 2017). The biogeochemical module was based on the carbon, silicate, and nitrogen ecosystem (CoSiNE) model (Chai et al., 2002; Xiu & Chai, 2014). The coupled ROMS-CoSiNE model customized for the Bohai Sea, Yellow Sea and East China Sea with a homogeneous 1/24° horizontal resolution (hereafter BYESbio24) has been applied to the study of hypoxia in the ECS (F. Zhou et al., 2017, 2020).

The setup of the BYESbio24 model is briefly reviewed. The curvilinear grid covered 117.5–132.0°E and 23.5–41.0°N. The s-coordinate terrain-following vertical grid had 30 levels. The flow field was initiated from a climatological January mean based on observations spanning from 1958 to 1987 (D. X. Chen, 1992) and driven by the climatological Comprehensive Ocean-Atmosphere Data Set (COADS; available at http://iridl.ldeo.columbia.edu/SOURCES/) forcings for 10 annual cycles to complete spin-up (F. Zhou et al., 2015). The climatological run output averaged in December was then used as the initial field for the continuous realistic run from 1998 to 2014. The daily-averaged outputs between 2009 and 2014 were analyzed in this study. The tidal constituents, including major diurnal and semidiurnal components, were derived from the OSU TPXO9-atlas (Egbert & Erofeeva, 2002). The 6-hourly wind field from the cross-calibrated multi-platform (CCMP; available at www.remss.com) ocean vector wind analysis product (Atlas et al., 2011; Mears et al., 2019; Wentz et al., 2015) was converted to the surface stress via the formula by Large and Pond (1981). The surface heat and freshwater fluxes were obtained from the European Centre for Medium-Range Weather Forecasts (ECMWF) ERA5 product (Hersbach et al., 2020; available at https://cds.climate.copernicus.eu/). The temperature, salinity, velocity and sea level elevation at open boundaries were nudged to the daily-mean HYbrid Coordinate Ocean Model (HYCOM; available at https://www.hycom.org) hindcast outputs (Bleck, 2002; Halliwell, 1998; Kelly et al., 2007). The CoSiNE model consisted of 13 state variables: nitrate, phosphate, silicate, ammonium, diatoms, picophytoplankton, microzooplankton, mesozooplankton, nitrogen-based organic detritus, biogenic silica detritus, DO, total CO_2, and total alkalinity. The ROMS and CoSiNE modules were coupled online, that is, all 13 ecosystem state variables were driven by real-time hydrodynamics. The model framework was elaborated by Chai et al. (2002) and Xiu and Chai (2014). The runoff and nutrient concentrations at the Datong hydrologic station in the lower reach of the Changjiang River were from the Changjiang Maritime Safety Administration (available at https://cj.msa.gov.cn/) and Ge et al. (2020), respectively. Details of the model setup process were described in F. Zhou et al. (2015), with further information on the detailed parameter setting and model validation for the ECS given in F. Zhou et al. (2017, 2020). An update of the model setup in this study is that the lateral and surface forcings were prescribed with newly-released OSU TPXO9-atlas, CCMP and ERA5 products.

In this study, the local biogeochemical oxygen consumption is integrated from the sediment-water interface to the pycnocline to obtain WOC:

$$\mathrm{WOC} = \int_{h}^{\mathrm{MLD}} (\partial_t \mathrm{DO} + \mathrm{DO}_{\mathrm{adv}} - \mathrm{DO}_{\mathrm{diff}})\mathrm{d}z, \tag{1}$$

where h is the seabed depth, MLD is the mixed layer depth, z is the vertical coordinate, ∂_tDO is the local change in the DO concentration, $\mathrm{DO}_{\mathrm{adv}}$ is the DO advection, and $\mathrm{DO}_{\mathrm{diff}}$ is the DO diffusion. The MLD is defined as the depth at which the potential density increases by $0.03\sigma_\theta$ from the surface following Sasaki et al. (2014). The WOC includes both the source term, that is, phytoplankton photosynthesis, and the sink terms, that is, respiration, remineralization and nitrification.

2.3.2. Benthic Model

The TOC-MAcrobenthos Interaction Model (TOCMAIM; W. Zhang & Wirtz, 2017; W. Zhang, Wirtz et al., 2019; W. Zhang et al., 2021) was used to quantify SOC. The core of the model is a mechanistic description of the early diagenesis processes of particulate organic carbon (POC), including sedimentation/erosion, burial, transport, degradation, and reworking by macrobenthos through uptake and bioturbation. The model resolves the mutual dependence of POC and macrobenthos as well as their vertical distributions in sediments impacted by the availability of DO. SOC is exclusively induced by POC degradation that varies along the sediment depth. The vertical distribution of the degradation rate is regulated not only by the quantity and quality of the POC but also by the availability of DO. DO is transported from the bottom water to sediments in three means: (1) Advection caused by porewater flows in permeable sediments. In reality, porewater is three-dimensional and regulated by migrating bedforms. In the model, an effective vertical flow velocity is estimated to quantify the net contribution of porewater flows to POC degradation. The porewater advective flux, F_{adv}, is used to represent its contribution to the total SOC. (2) Molecular diffusion (i.e., Brownian motion) driven by the DO gradient and regulated by sediment porosity, tortuosity and ambient temperature. Its contribution to the total SOC is denoted by the molecular diffusive flux, F_{mol}. (3) Bioturbation, by macrobenthos, through mixing and burrow ventilation in both permeable and impermeable sediments (Meile & Van Cappellen, 2005; Meysman et al., 2006; Middelburg, 2018; Santos et al., 2012). Benthic fauna have long been recognized for their central role in reworking solutes and particles in sediment (Griffiths et al., 2017; Meile & Van Cappellen, 2005; Middelburg, 2018; Snelgrove et al., 2018; W. Zhang, Wirtz, et al., 2019). It is modeled by an effective diffusive process in TOCMAIM. The bioturbation-induced oxygen consumption by degradation of POC in deeper sediments is represented by the bioturbation diffusive flux, F_{bio}. The effective bioturbation diffusivity takes into account the mixing and bio-ventilation impact on the solute. In summary, the SOC is a sum of the three terms:

$$\mathrm{SOC} = F_{adv} + F_{mol} + F_{bio}. \quad (2)$$

The theoretical basis, mathematical descriptions, sensitivity analysis of model parameters and model uncertainties associated with the benthic oxygen dynamics were elucidated in W. Zhang et al. (2021).

The survey data for sediment grain size, sediment types (mud/sand), TOC and TN (Table 2) were used to initialize the benthic model, and the model was then spun up to achieve an equilibrium distribution in terms of macrobenthos biomass (W. Zhang, Wirtz, et al., 2019). Then, the pelagic model exported bottom current velocity, bottom shear stress, bottom temperature, bottom DO, and bottom detritus in the form of POC to the benthic model to simulate realistic years. Nitrogen-based organic detritus was converted to POC via the Redfield ratio (Redfield, 1934). The uniform horizontal grid size was ~4 km, and the vertical resolution was 1 cm within the 30 cm-thick surface sediment.

3. Results

3.1. Model Validation

Stratification is essential for sustaining hypoxia. Therefore, special attention has been given to the properties within surface and bottom waters. The model outputs for daily-averaged sea surface temperature (SST) were compared with the NOAA OI SST V2 high resolution dataset provided by the NOAA/OAR/ESRL PSD (Reynolds et al., 2007; available at https://psl.noaa.gov/dat/gridded/data.noaa.oisst.v2.highres.html). The Pearson correlation coefficient between the simulated and observed results for the mean temperature over the ECS from 2009 to 2014 was 0.997 (Figure 3a). This result suggests that the model reproduced the multiscale variation in SST well. The Taylor diagrams for comparisons between the model outputs and the measurements at the 31°N transect (Table 2) in terms of bottom temperature and salinity are shown in Figures 3b and 3c, respectively. Although both temperature and salinity vary over a wide range, Figures 3b and 3c show that the differences between simulations and observations are mostly within one normalized standard deviation (SD), while the correlation coefficients are high at the significance level of 0.05. This result suggests that the model reproduced the temperature and salinity in bottom water well. Algal blooms fueled oxygen depletion in subsurface water. Chlorophyll-a (Chl-a) concentration is a proxy for phytoplankton biomass. Monthly-averaged surface Chl-a concentrations over the ECS from a locally modified Chl-a (LMC) dataset (Hao et al., 2019), which was calibrated by the ship-measured Chl-a

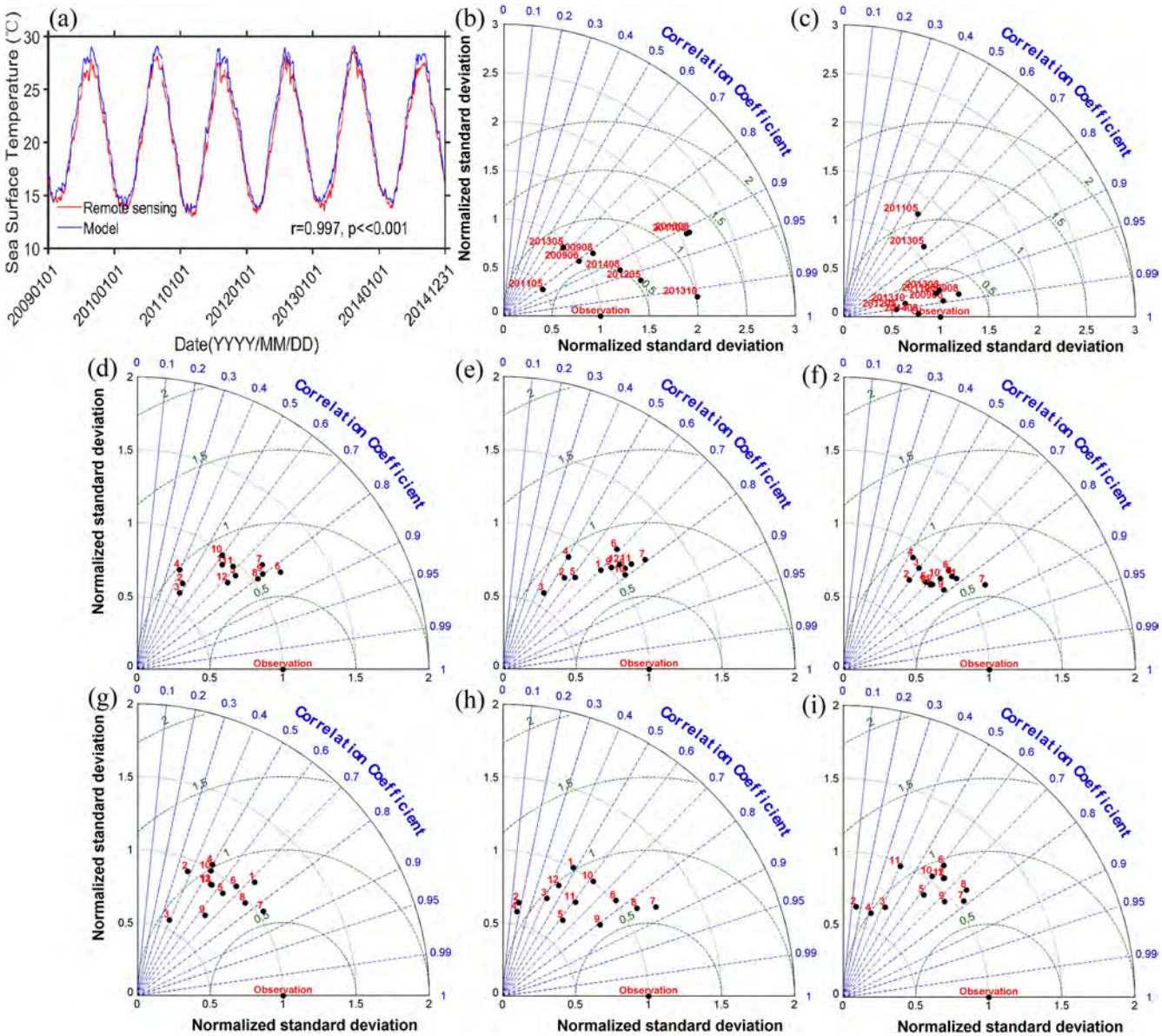

Figure 3. (a) Averaged daily-mean SST in the study area from NOAA High Resolution SST data (red line) and the model output (blue line) versus date. The Pearson correlation coefficient between the two datasets, *r*, is exhibited in the figure, as well as the *p*-value (*p*). Taylor diagrams are used to compare between the model outputs and the measurements (designated as 'Observation') synthetically taking into account model SDs normalized by SDs of observations (the radial distances from the origin), the correlation between the modeled results and observation (the azimuthal position), the normalized root-mean-square error (RMSE; the distance to the 'Observation' point). The modeled bottom temperature and salinity at the 31°N transect are compared to the observations in (b) and (c), respectively. The daily-mean model outputs grouped according to measurements by distinct cruises shown in Table 2 are designated by their year and month in the form of YYYY/MM. The Taylor diagrams for the monthly-averaged Chl-a from the model and the locally modified Chl-a dataset by Hao et al. (2019) from 2009 to 2014 are shown in (d)–(i), respectively. Red numbers in (d)–(i) denote months.

concentration in the ECS, were used to validate the model. The Taylor diagrams in Figures 3d–3i demonstrate the good performance of the model in simulating the surface Chl-a.

Both the DO concentration and the hypoxic zone off the CE could vary dramatically in only a number of days (W. Zhang et al., 2018; F. Zhou et al., 2017). To make full use of the available observational data to evaluate the simulation, two field datasets were used for comparison. In the first dataset, the measured bottom DO at the 31°N transect was compared with the daily-averaged model output on the day when measurement was implemented. The data were grouped according to their year and month in the Taylor diagram (Figure 4a). Figure 4a suggests a good performance of the model in simulating the bottom DO, particularly in summer. In the second dataset, the

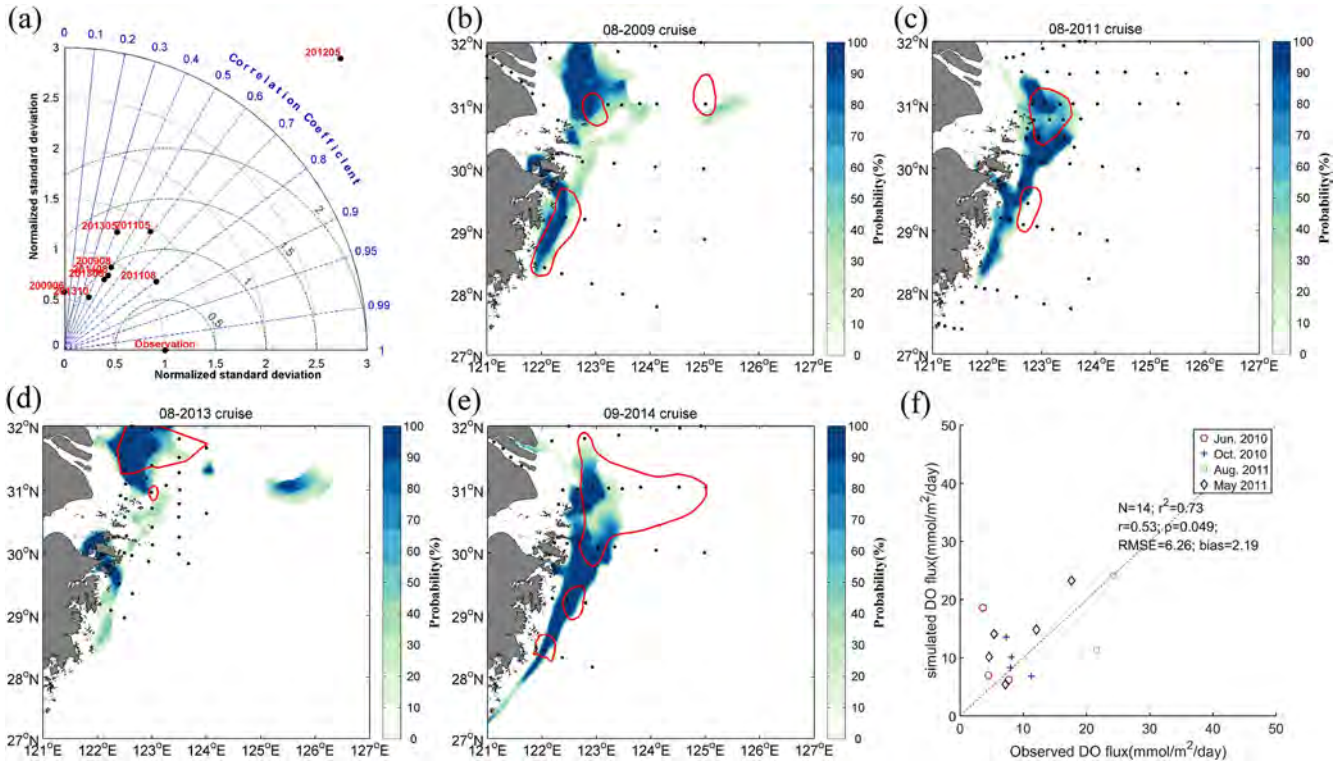

Figure 4. (a) The Taylor diagrams for comparisons between the model outputs and the measurements (designated as 'Observation' in the figure) at the 31°N transect in terms of the bottom DO. The cruise data in Table 2 are designated by their year and month in the form of YYYY/MM. (b–e) Contour plots are for probabilities of hypoxia occurring during the cruise durations in the model; red lines are for hypoxia extents extracted from ship-borne surveys; black spots are for survey stations. (b) Cruise from August 13, 2009 to August 31, 2009; (c) cruise from August 14, 2011 to August 27, 2011; (d) cruise from August 17, 2013 to August 26, 2013; (e) cruise from August 21, 2013 to September 15, 2014. (f) Point-to-point comparisons between the model outputs and the observations in terms of the SOC. The number of samples (N), coefficient of determination (r^2), Pearson correlation coefficient (r), p-value (p), RMSE and bias are exhibited in the figure.

hypoxic zones extracted from four ship-borne surveys were compared with the model estimated probabilities of hypoxia occurring during the cruise period (Figures 4b–4e). The model captured the hypoxic zone well in the 4 yr except for a tongue-shaped hypoxic zone between Region III and Region V in 2014.

Observational data for SOC, as shown in Table 2, were compared with the monthly-averaged simulated results in Figure 4f. The sediment cores were incubated in the absence of physical disturbances. Therefore, the incubation measurement was compared to the summation of the molecular diffusive flux and the bioturbation diffusive flux from the model. Cai et al. (2014) suggested that their method took into account both the advective and diffusive fluxes across the water-sediment interface. Therefore, the measurement by the $^{224}Ra/^{228}Th$ disequilibrium method was compared to the simulated total flux. Figure 4f shows an overall good performance of the model in reproducing the SOC. The comparisons at each station are shown in Figures S1a–S1n in Supporting Information S1. The largest deviation between the modeled and observed values occurred in Region II. The overestimation (bias = 2.19 mmol/m^2/day in Figure 4f) was partly due to the one-way coupling between the pelagic and benthic models without feedback from the benthic model.

A critical state variable relevant to benthic oxygen dynamics that can be directly compared to field data is macrobenthos biomass. A general agreement is shown between the measured and simulated macrobenthos biomass (Figure 5a). Both field observations (Figure 5b) and simulation results (Figure 5c) showed a clear difference in biomass between areas with and without the impact of seasonal hypoxia. Biomass was significantly smaller in areas that were subject to seasonal hypoxia than in those not affected by hypoxia (Figure 5b). It is particularly worth noting that macrobenthos were mainly characterized by deposit feeders (including surface and sub-surface deposit feeders, with the latter most dominant) in areas subject to seasonal hypoxia, while the diversity was higher in areas without hypoxia (Figure 5d).

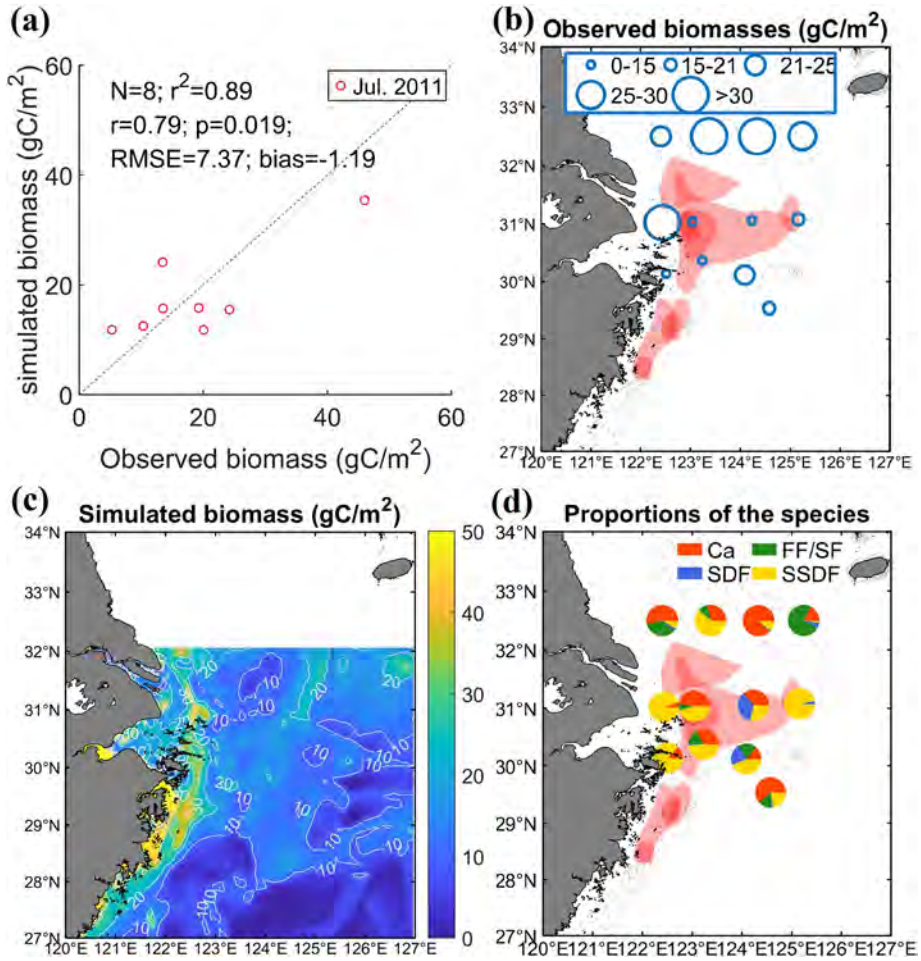

Figure 5. (a) Point-to-point comparison between the sampled macrobenthos biomasses at stations south of 32°N and the simulated results. The number of samples (N), coefficient of determination (r^2), Pearson correlation coefficient (r), p-value (p), root-mean-square error (RMSE) and bias are exhibited in the figure. (b) Ash-free dry weight macrobenthos biomasses at the sampling stations collected by the cruise in July 2011. Red patches are for hypoxia extents extracted from ship-borne surveys. Isobaths are plotted by dashed gray lines in units of meters. (c) Monthly averaged macrobenthos biomass in July 2011 derived from the model. (d) Pie charts for community compositions based on the following classification criteria: carnivores (Ca), surface-deposit feeders (SDF), subsurface-deposit feeders (SSDF), suspension feeders (SF), filter feeders (FF). Red patches are for hypoxia extents extracted from ship-borne surveys. Isobaths are plotted by dashed gray lines in units of meters.

3.2. Spatiotemporal Variations in the SOC

The total SOC exhibited quite similar patterns in August of 2009, 2011, 2013 and 2014, although the hypoxic zones differed substantially (Figures 6a–6d). There are several zones with high SOC in summer, that is, CSD (within Region I), TSS (within Region II), ZMCMB (within Region IV), SWCIM (within Region V) and outer shelf (approximately deeper than 100 m within Region VI). In the core hypoxic zone (Region III), the total SOC was constantly low (Figures 6a–6d). In contrast, the SOC was high in Region IV, where hypoxia also often occurred (Figures 6a, 6b and 6d). In 2013, the hypoxic zone was shifted to the north of 31°N expanding on the Changjiang bank, but the SOC pattern did not change much (Figure 6c). The standard deviation was derived from the daily variation with respect to the monthly mean, which reflects the synoptic variability. Figures 6e and 6f show that the synoptic variation was strong where the mean flux was high.

The total SOC exhibited distinct temporal variation characteristics among different regions. Overall, the annual mean SOC in Region II was the highest among all regions (Figures 7a–7f). The seasonal variation in Region I exhibited a sinusoidal shape (Figure 7a). The total SOC in Region II dropped abruptly in summer, while it stayed

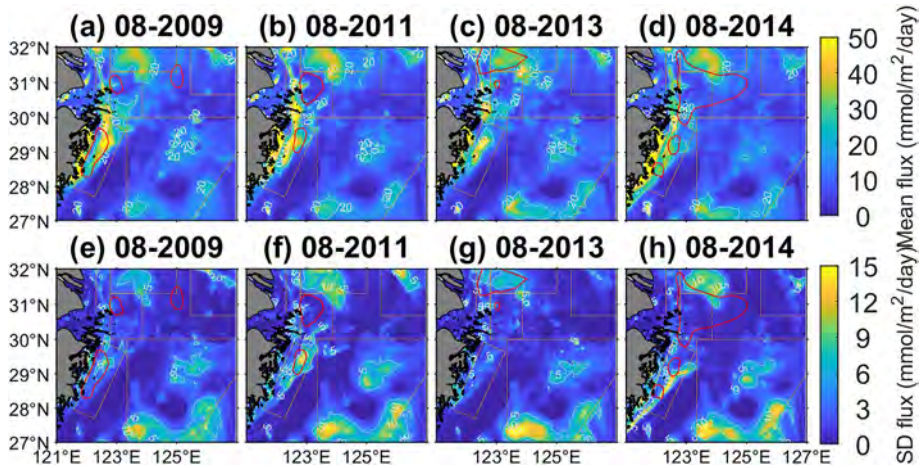

Figure 6. Monthly-mean total SOC in August of 2009 (a), 2011 (b), 2013 (c), and 2014 (d). SD of total SOC calculated from the daily-mean model outputs in August of 2009 (e), 2011 (f), 2013 (g), and 2014 (h). Six study regions are specified by orange polygons. Red lines are for hypoxia extents extracted from ship-borne surveys.

on a plateau in other seasons (Figure 7b). The porewater advective flux in Region II reached a trough in summer, while it reached a peak in winter (Figure S10b in Supporting Information S1). The total SOC in Region III experienced a pulse in summer but stayed low in the other seasons (Figure 7c), while the porewater advective flux in Region III was low in summer and high in winter (Figure S10c in Supporting Information S1). The total SOC in Regions IV and V, dominated by the bioturbation diffusive DO flux (Figures S9d and S9e in Supporting Information S1), had rich intraseasonal, interseasonal and interannual variations (Figures 7d and 7e). In Region VI, it was difficult to distinguish an annual cycle with significant seasonality (Figure 7f). The monthly-mean flux and the SD in that month seemed to correlate well (Figures 7a–7f). In particular, the SD in Region II was the highest among the six studied regions.

The distributions of the benthic porewater advective DO flux on the ECS shelf in August of 2009, 2011, 2013 and 2014 are illustrated in Figures 8a–8d, respectively. The results suggest that a coarser median grain size permits a higher porewater advective DO flux (Figure 2a). Porewater advective DO flux was high on the TSS (Region II)

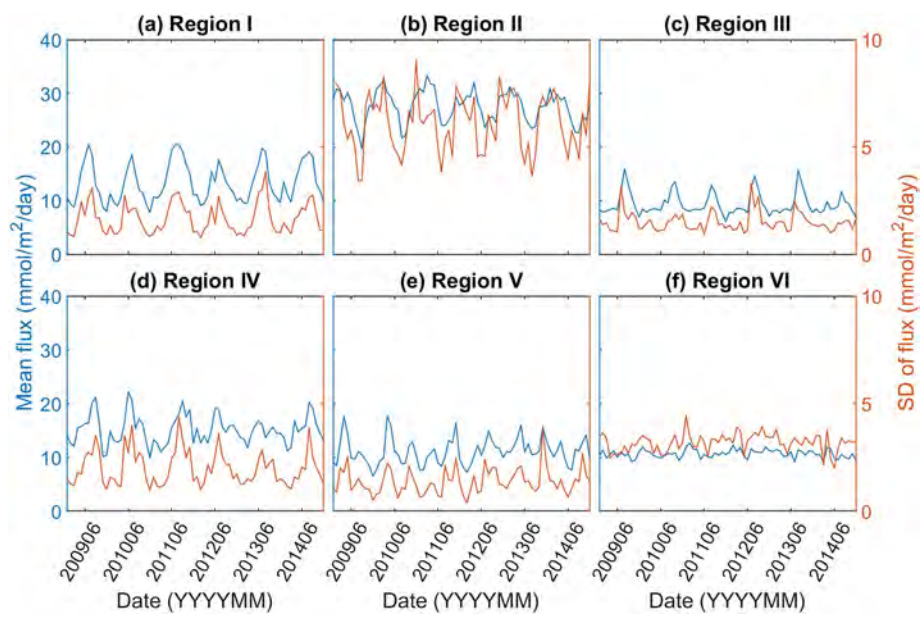

Figure 7. Regional-mean of monthly-mean total SOC versus its month from Region I (a) to Region VI (f). The regional-mean SD of the total SOC calculated from the daily-mean model outputs in a month is also plotted in each panel.

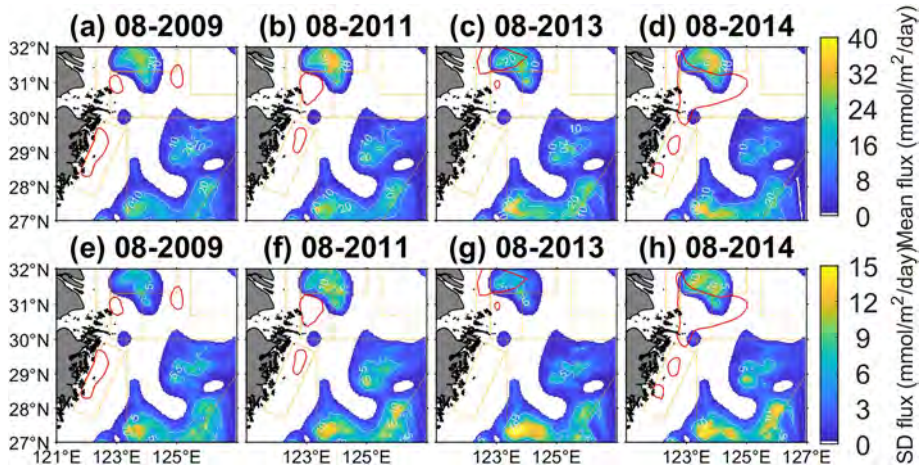

Figure 8. Monthly-mean porewater advective DO flux across the water-sediment interface in August of 2009 (a), 2011 (b), 2013 (c), and 2014 (d). SD of porewater advective DO flux calculated from the daily-mean model outputs in August of 2009 (e), 2011 (f), 2013 (g), and 2014 (h). Six study regions are specified by orange polygons. Red lines are for hypoxia extents extracted from ship-borne surveys.

and RSA (Region VI) with large grain sizes (Figures 2a and 8a–8d). In contrast, porewater advective DO fluxes were extremely weak on muddy sediments where mud depocenters were located, that is, Regions I, IV and V, which was consistent with the findings in the North Sea (W. Zhang et al., 2021). In 2009, 2011 and 2014, hotspots of advective flux (surrounded by the 10 mmol/m^2/day contour line) on the TSS were adjacent to but hardly overlapped with the hypoxic zone (Figures 8a, 8b and 8d). However, in 2013, the hotspots of advective flux on the TSS overlapped with a large portion of the hypoxic zone (Figure 8c). Figures 8e, 8f, 8g and 8h show that synoptic variation was strong (~30% of the mean flux) where the porewater advective DO flux was high.

Macrobenthos plays a significant role in reworking the OC and regulating the SOC (W. Zhang, Wirtz, et al., 2019; W. Zhang et al., 2021). In the case that the molecular diffusive flux is minor (Figures S6 & S7 in Supporting Information S1), several results can be found by comparing Figures 6 and 8. The porewater advective flux and the bioturbation diffusive flux were comparable on the ECS shelf. It appeared that the bioturbation diffusive flux was high where the porewater advective flux was low except at the submerged river valley where both fluxes were low. In other words, the sediment type was closely correlated with the predominant term. Permeable sandy sediment was favorable for porewater advective flux rather than bioturbation diffusive flux (Figures 2a and 2b). Muddy sediment was favorable for the bioturbation diffusive DO flux (Figures 2a and 2b). At the mud depocenters, the permeability was so low that the porewater water advective DO flux was almost null (Figure 8). Furthermore, the bioturbation diffusive fluxes differed among the mud depocenters (Figure S8 in Supporting Information S1) This was probably due to the difference in the freshness of the sedimentary POC, which was closely related to local primary production and transport (W. Zhang et al., 2015). The bioturbation diffusive DO fluxes in the CSD (Region I) and the ZMCMB (Region IV) were higher than those in the SWCIM (Region V), particularly in summer (Figures S9a, S9d and S9e in Supporting Information S1), suggesting that the high primary productivity in coastal waters facilitated the higher bioturbation diffusive DO flux due to the freshly deposited POC.

3.3. SOC Versus WOC

The results shown in Figures 9a–9d indicate that the WOC in coastal waters was consistently high. The interannual variation in the high WOC area, to some extent, was synchronized with the interannual variation in the hypoxic zone. For example, in 2013, when the hypoxic zone was located more northerly than usual, the whole high WOC area (≥~100 mmol/m^2/day) shifted more northward than those in 2009, 2011 and 2014 (Figures 9a–9d). The SD in August was normally strong in coastal hypoxic zones (Figures 9e, 9f and 9h). In particular, the relatively weak SD of WOC in the hypoxic zone to the north of 31°N in 2013 suggests persistently high WOC in a relatively mild hydrographic environment (Figure 9g).

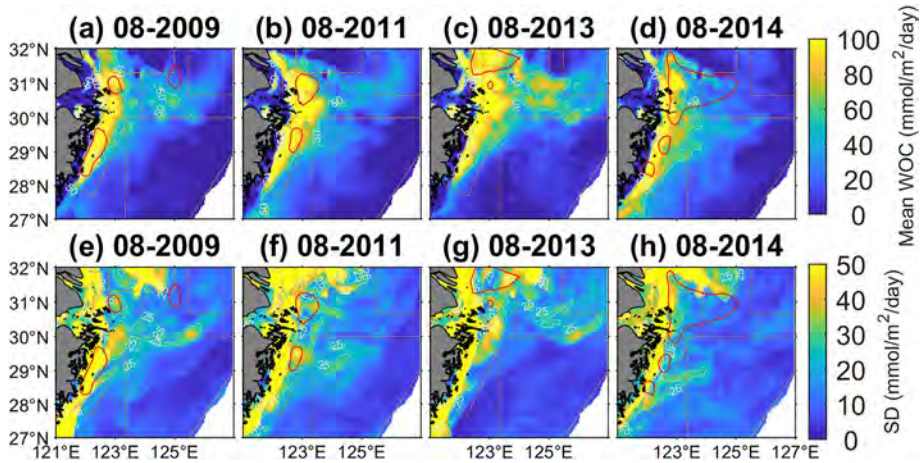

Figure 9. Monthly-mean WOC in August of 2009 (a), 2011 (b), 2013 (c), and 2014 (d). SD of WOC calculated from the daily-mean model outputs in August of 2009 (e), 2011 (f), 2013 (g), and 2014 (h). Six study regions are specified by orange polygons. Red lines are for hypoxia extents extracted from ship-borne surveys.

Overall, the monthly-mean WOC was much higher than that of the SOC in coastal waters in summer (Figures 7a–7f and 10a–10f). The synoptic variability of WOC was positively correlated with the monthly-mean value and one-order higher than that of the SOC (Figures 7a–7f and 10a–10f). There were distinct annual cycles with seasonality in WOC in all regions (Figures 10a–10f). The interannual variation of WOC was also obvious. Taking the summer hypoxia event in 2013 as an example, the WOC in Regions IV was much lower those in other years (Figure 10d); in contrast, the WOC in Regions I, II and III in the summer of 2013 was exceptionally high (Figures 10a–10c).

The ratio between SOC and the summation of SOC and WOC was used to quantify the relative contribution of SOC to total local DO consumption. The results shown in Figures 11a–11d indicate four high-value zones in terms of SOC/(SOC + WOC) in August on the ECS shelf, that is, TSS (Region II), ZMCMB (Region IV), SWCIM (Region V) and RSA (Region VI). The contribution of SOC to the total local DO consumption within the hypoxic zone in Region IV is generally above 0.2 but lower than 0.4. Another distinct feature was that the

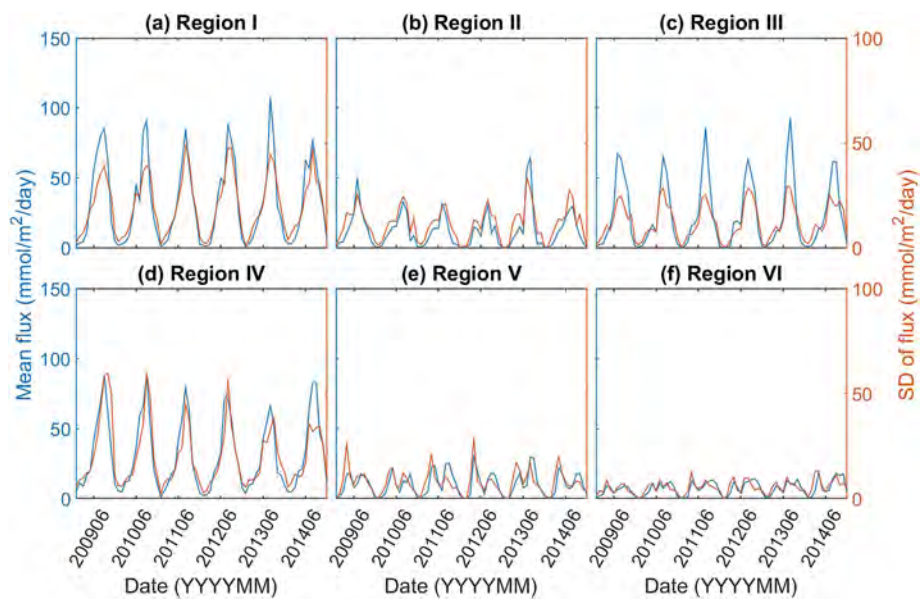

Figure 10. Regional-mean of monthly-mean WOC versus its month from Region I (a) to Region VI (f). The regional-mean of SD of WOC calculated from the daily-mean model outputs in a month is also plotted in each panel.

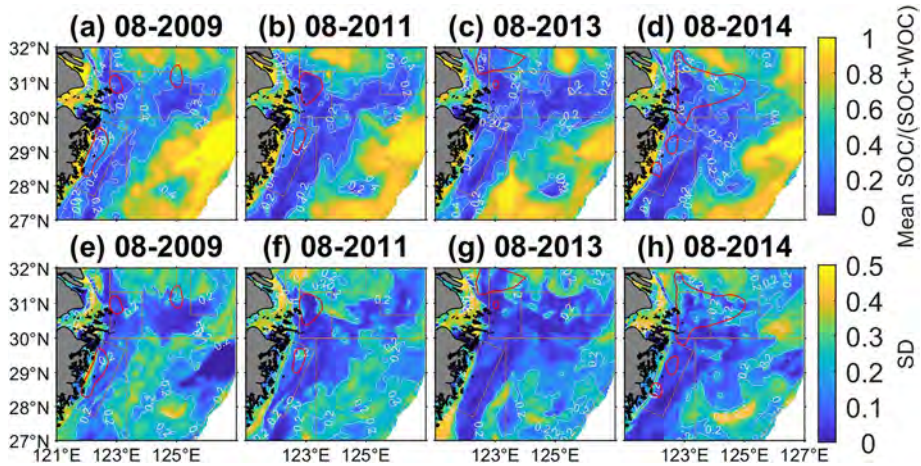

Figure 11. Monthly-mean SOC/(SOC + WOC) in August of 2009 (a), 2011 (b), 2013 (c), and 2014 (d). SD of SOC/(SOC + WOC) calculated from the daily-mean model outputs in August of 2009 (e), 2011 (f), 2013 (g), and 2014 (h). Six study regions are specified by orange polygons. Red lines are for hypoxia extents extracted from ship-borne surveys.

SOC/(SOC + WOC) in Region III was persistently low (below 0.2) in August (Figures 11a–11d). When the hypoxic zone expanded into Region II in 2013, the SOC/(SOC + WOC) dropped significantly from ~1 in other years to approximately 0.2–0.4. The SD of SOC/(SOC + WOC) in August also varied significantly in different years, suggesting a large deviation when sampling in different years (Figures 11e–11h).

Distinct annual cycles with significant seasonality existed in terms of SOC/(SOC + WOC) in all regions, which varied in a wide range between 0.2 and 1 (Figures 12a–12f). Another common feature was that the peak values occurred exclusively in winter, and some large intraseasonal variations could also be found from the time series. Another fact is that no evident correlation between the synoptic variability and the monthly mean can be found (Figures 12a–12f).

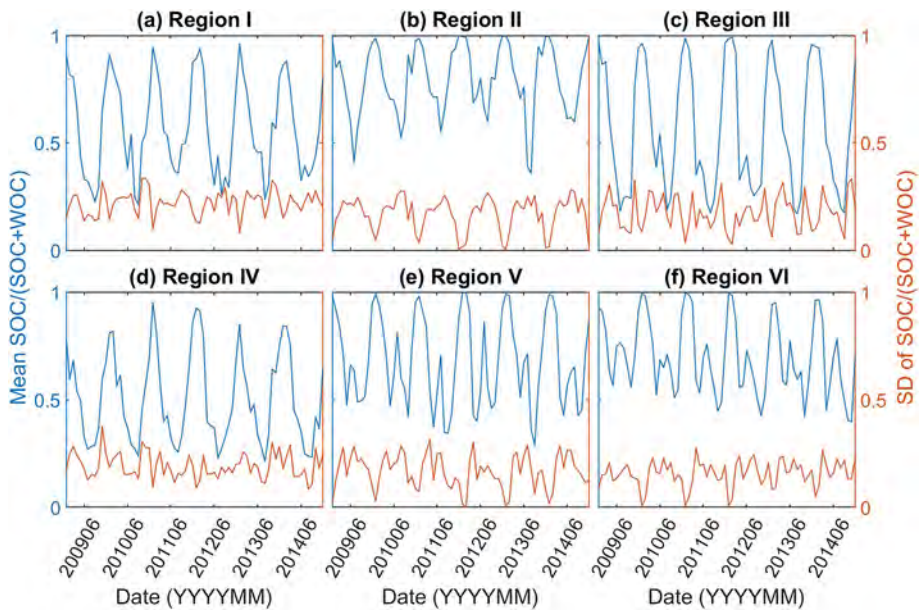

Figure 12. Regional-mean of monthly-mean SOC/(SOC + WOC) versus its month from Region I (a) to Region VI (f). The regional-mean SD of SOC/(SOC + WOC) calculated from the daily-mean model outputs in a month is also plotted in each panel.

4. Discussion

4.1. Major Driver of the Variation of Hypoxia

In boreal summer (June to August), the interannual variation ranges of monthly-averaged SOC/(SOC + WOC) were within [∼20%, ∼50%], [∼35%, ∼80%], [∼15%, ∼55%] and [∼20%, ∼40%] in Regions I–IV, respectively (Figures 12a–12d). It is worth noting that in the hypoxic zone, the SOC/(SOC + WOC) was lower than the regional mean (Figures 11a–11d). In August 2013, when the hypoxic zone expanded on the Changjiang bank into Region II, the monthly-averaged SOC/(SOC + WOC) in Region II dropped to ∼35% (Figure 12b). By comparing Figures 6a–6d and 9a–9d, it is more evident that the hypoxic zone coincided with the high WOC patches rather than the high SOC patches. Therefore, it is concluded that WOC is the major driver of the variation of hypoxia on the ECS shelf.

It is of interest to find a rule of thumb for identifying the relative contribution of SOC to hypoxia compared to WOC in estuaries and shelf seas. Via cross-system comparison of several typical hypoxic zones in estuaries and river-dominated shelf seas, the contribution of SOC tends to be larger in shallower systems because more sinking organic detritus reaches the seafloor (Fennel & Testa, 2019; Kemp et al., 1992). For example, hypoxia in the Pearl River estuary and northern Gulf of Mexico was believed to be very sensitive to SOC, and hypoxia is characterized by a thin layer above the seabed (Fennel et al., 2013; L. Yu et al., 2015; H. Zhang & Li, 2010). However, Fennel and Testa (2019) showed that the estimated SOC contribution to the total local oxygen consumption in the ECS was exceptionally lower than the prediction by Kemp et al. (1992). One reason to explain the discrepancy from the hypothesis might be attributed to the strong tidal current in the ECS, particularly on the Changjiang bank, which facilitates the resuspension of POC (Luo et al., 2017; Xuan et al., 2016). Furthermore, the energetic hydrodynamics sustain the transport of nutrients and POC (Meng et al., 2020; F. Zhou et al., 2020). This suggests that the specific hydrodynamic characteristics should also be taken into account when assessing the contribution of SOC versus WOC to hypoxia.

We found WOC also as the major driver of the temporal variation in SOC/(SOC + WOC) over the ECS shelf. Firstly, the seasonal variation in SOC/(SOC + WOC) is dominated by the variation in WOC (Figures 12a–12f). In each sub-region, SOC/(SOC + WOC) reached a peak in winter, but normally stayed low in summer (Figures 12a–12f). This is because the WOC was high in summer but extremely low in winter (Figures 10a–10f), while the SOC varied in a relatively narrow range. A strong synoptic variation in WOC (Figures 10a–10f) further makes the estimation of the overall contributions of SOC and WOC to hypoxia solely by field measurements difficult and often inconsistent among studies (Chi et al., 2021; Ni et al., 2016; Song et al., 2016; B. Wang et al., 2017; H. Zhang et al., 2017; Zhao et al., 2018; Zhu et al., 2016).

The seasonal dynamics of the benthic system should also be paid attention to. The SOC is closely related to the early diagenesis of organic carbon. In Region II, the lower SOC in summer and higher SOC in winter (Figure 7b) suggest an overall lower POC degradation rate in summer than in winter in the Changjiang bank sediments. This finding is supported by recent field measurements by L. Wei et al. (2021). In summer, the DO in the bottom water is lower and the porewater advection transporting oxygen into deeper sediments is weaker due to the milder hydrographic environment (in terms of wind-waves and wave-current interaction) than that in winter. This results in lower POC degradation rate associated with porewater flows in summer in permeable sandy sediments such as the Changjiang bank. On the other hand, because of abundant food supply and favorable temperature in late spring and summer, benthic fauna grow to their maximum body size and bioturbation reaches to a peak in summer. This results in a higher POC degradation rate associated with bioturbation in summer especially in impermeable muddy sediments (W. Zhang et al., 2021). However, formation of hypoxia would lead to death or escape of macrobenthos which subsequently deteriorates the functioning of benthos in mediating SOC.

4.2. How the Coupled Pelagic-Benthic Processes Mediate Hypoxia in Non-Depositional Areas

Results from the coupled pelagic-benthic model provide insights into the variability of driving mechanisms of hypoxia formation among different regions and years. A particular phenomenon occasionally observed is a northward shift of the hypoxic zone to non-depositional areas, for example, a large hypoxic zone north of 31°N

expanded onto the Changjiang bank in 2013 (Figure 1). Figure 12b shows that SOC/(SOC + WOC) in Region II, which partly overlaps with the Changjiang Bank, dropped significantly in the summer of 2013. Figure 10b shows that the summer WOC in Region II was exceptionally high in 2013. However, the SOC in Region II in 2013 was not abnormal (Figure 7b). A look into the benthic components indicates that both the molecular diffusive DO flux and the bioturbation-induced DO flux in the summer of 2013 were higher than those in other years (Figures S7b and S9b in Supporting Information S1). In contrast, the porewater advective DO flux in the summer of 2013 was exceptionally lower than that in other years (Figure S10b in Supporting Information S1). By plotting the three terms together in Figure 13a, it can be seen that the variation in the porewater advective DO flux dominated the variation in the total SOC in Region II. The decline in the porewater advective DO flux in summer offset the increments in the bioturbation diffusive DO flux and the molecular diffusive DO flux.

The abovementioned benthic responses are largely attributed to the less-energetic hydrodynamics in the summer of 2013 in Region II than those in other years of this study. Similar to the resuspension of sediment on the Changjiang bank (Luo et al., 2017; F. Zhou et al., 2020), tide-induced bottom currents dominate the resuspension of POC in Region II. Luo et al. (2017) argued that due to the small seasonal difference in the tide, particle plumes in the bottom water should exhibit quite similar distributions between winter and summer. However, our results suggest that the benthic-pelagic coupling and associated biogeochemical processes can be quite sensitive to hydrodynamic forcing that is superimposed to the regular tides. The SST in August 2013 in Region II was higher than those in 2009, 2011 and 2014 (Figure 13b). This phenomenon was also found by Yan et al. (2020) for the entire ECS and Yellow Sea, and the higher SST was due to the enhanced solar radiation and weakened wind. The higher surface and bottom temperature difference shown in Figure 13b suggests that the stratification in August 2013 was stronger than those in other years. This further, to some extent, suggests a milder hydrographic environment in August 2013. Stormy processes could induce much stronger bottom currents than tidal currents (Luo et al., 2017). Annual typhoon tracks until the end of August in 2009, 2011, 2013 and 2014 were collected from the western North Pacific TC database created by the China Meteorological Administration (Lu et al., 2021; Ying et al., 2014; available at https://tcdata.typhoon.org.cn/zjljsjj_zlhq.html; Figures 13c–13f). In 2013, no typhoons entered the Yellow Sea, and it appears that the tracks were suppressed to the southeast of Region II. Therefore, Region II was less affected by episodic strong-wind events in the summer of 2013. On one hand, the weaker bottom current resulted in a reduction in the porewater advective DO flux in the summer of 2013. On the other hand, the exceptionally mild hydrographic environment and enhanced solar radiation favored high primary production and the subsequent high WOC (Figure 10b). The higher molecular diffusive DO flux in the summer of 2013, indicating more DO produced in the water column, supports the conjecture above. Both higher primary production and less energetic hydrodynamics are favorable for a larger bioturbation diffusive flux before the formation of hypoxia. However, the increment in bioturbation diffusive DO flux was unable to overcome the decline in the porewater advective DO flux. This result suggests that the change in hydrodynamics could trigger complex responses in the coupled pelagic-benthic system, and those interactions should be taken into account to increase predictive skill for forecasting hypoxia events.

We believe that the abovementioned benthic-pelagic coupling is applicable to other coastal shelf seas where hypoxia occurs on permeable sandy sediments. A general understanding can be obtained thereby, that is, a larger contribution of SOC to hypoxia and more DO depletion on permeable sediments correspond to stronger wind mixing and weaker solar radiation, and the opposite is true when wind mixing becomes weaker and solar radiation gets stronger (Figure 14). The former is associated with a deeper mixed layer and lower primary productivity as well as higher porewater advection-induced DO flux, whilst the latter is associated with a shallower mixed layer and higher primary productivity as well as higher bioturbation diffusive DO flux.

4.3. Model Limitation and Future Work

Uncertainties of our simulation results may originate from the one-way coupling between the benthic and pelagic models apart from simplification in model formulation and parameterizations for complex ecological processes. In one-way coupling, the feedback of oxygen transport in subsurface sediments caused by bioturbation and porewater flows (estimated by TOCMAIM) to the near-bottom pelagic oxygen concentration (calculated

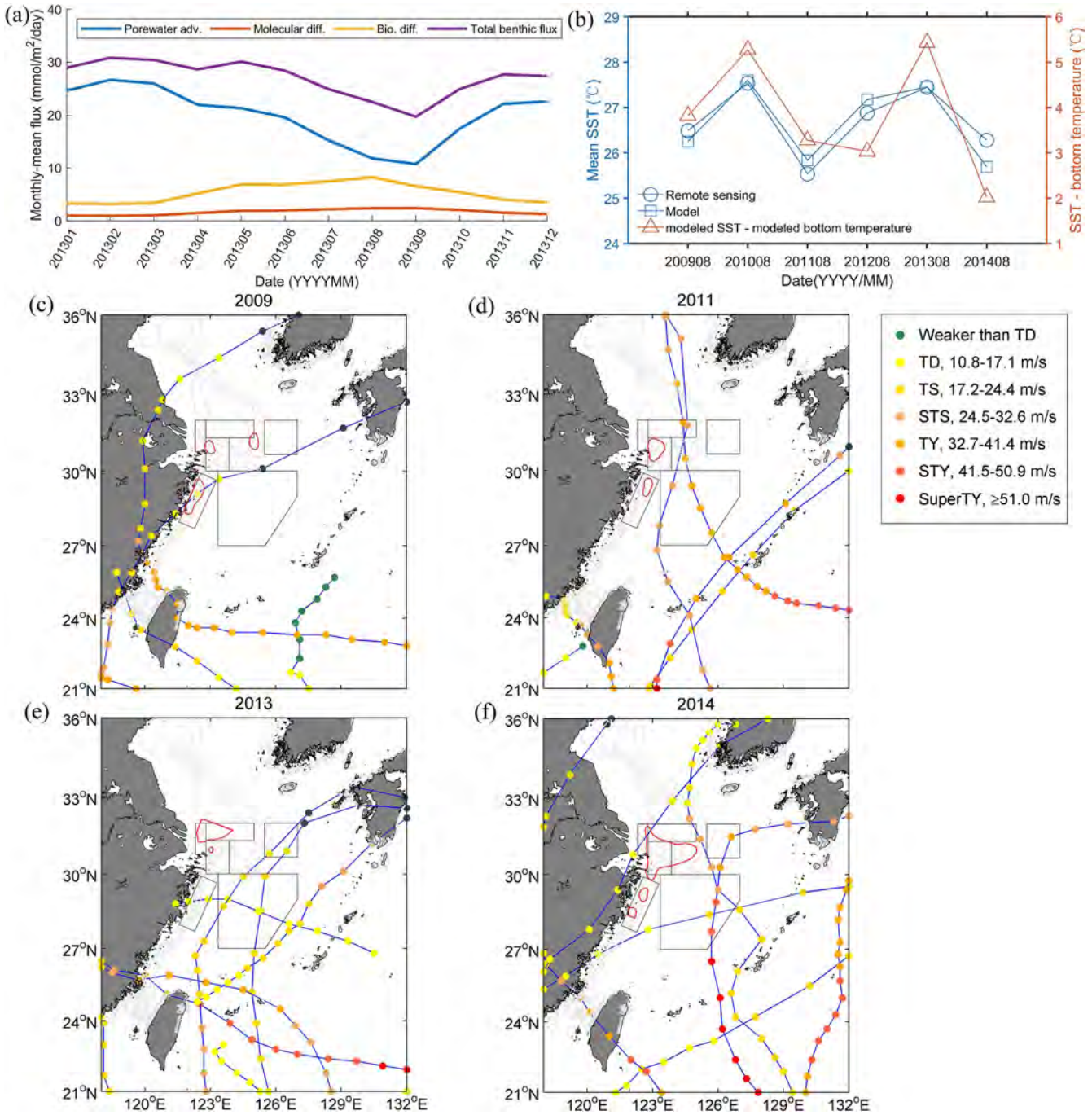

Figure 13. (a) Regional-mean of monthly-mean porewater advective DO flux, molecular diffusive DO flux, bioturbation diffusive DO flux and total SOC in Region II in 2013. (b) Regional-mean monthly-mean SST and temperature difference between surface and bottom waters in Region II in August from 2009 to 2014. SST data were derived from the NOAA OI SST V2 High resolution dataset and the BYESbio24 model. The temperature differences were derived from the BYESbio24 model. (c–f) Annual typhoon tracks until the end of August in 2009, 2011, 2013, and 2014 derived from the western North Pacific TC database created by the China Meteorological Administration. The typhoon strength is classified by the maximum wind speed near the center denoted by dots in different colors. TD: tropical depression; TS: tropical storm; STS: severe tropical storm; TY: typhoon; STY: severe typhoon; SuperTY: Super typhoon. Six study regions are specified by black polygons. Red lines are for hypoxia extents extracted from ship-borne surveys.

by ROMS-CoSiNE) was missing. This resulted in an overestimation of the SOC (bias = 2.19 mmol/m^2/day in Figure 4f). However, it did not qualitatively affect the conclusion that the SOC was not the major driver causing hypoxia on the ECS shelf in summer, which was also pointed out by J. Zhou et al. (2021). As hypoxia degenerated

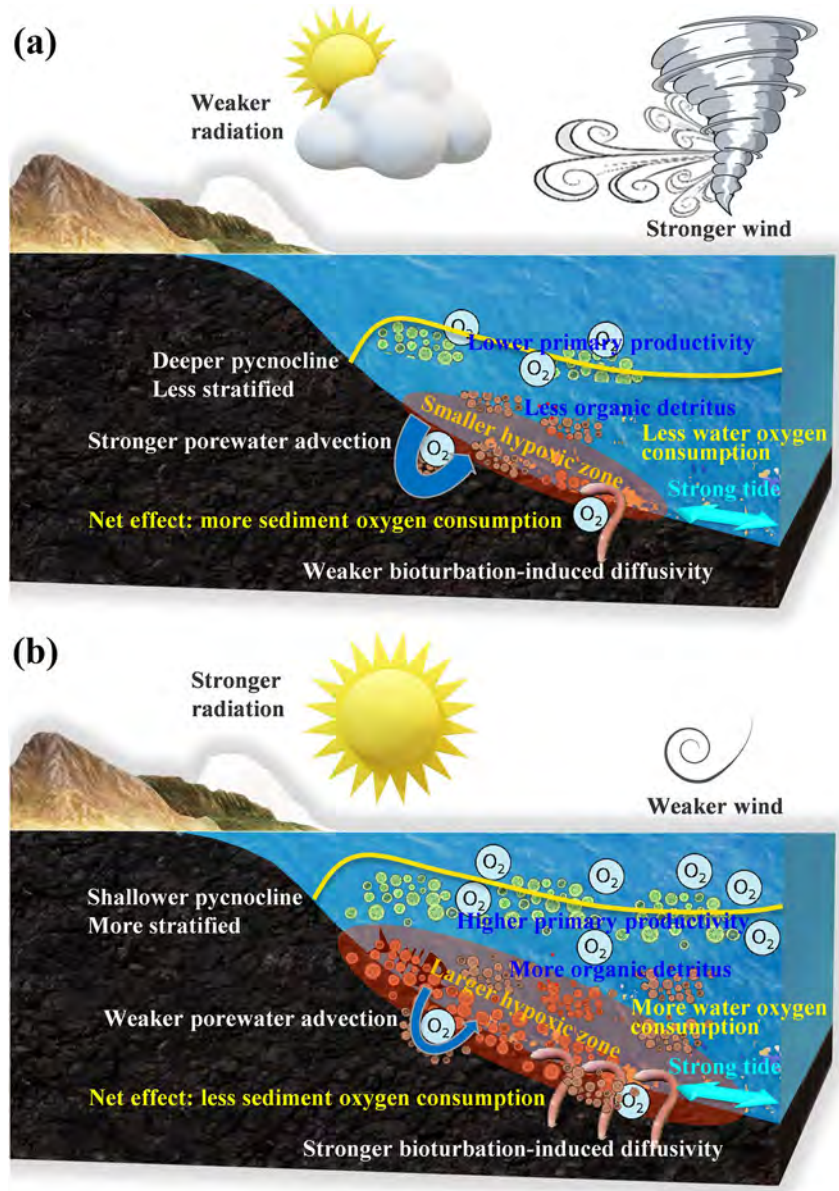

Figure 14. Schematic diagrams of coupled pelagic-benthic responses to a more disturbed hydrographic environment (a) and a milder hydrographic environment (b) in a coastal shelf sea with permeable sediment subject to hypoxia.

to anoxia (approaching null conditions), the overestimation of SOC by the model sharply increased as indicated by Figure 4f. A two-way online coupling between the benthic and pelagic models would better capture the feedback of SOC to the pelagic DO budget, allowing us to reproduce the extreme condition.

Modeling the responses of infaunal macrobenthos to hypoxic or even anoxic conditions involves uncertainties from sophisticated biogeochemical processes and human-induced disturbance (Briggs et al., 2017; Levin et al., 2009). The TOCMAIM model estimates macrobenthic biomass as well as its vertical distribution by resolving the impact of POC (in terms of quality and quantity) and oxygen on the growth of macrobenthos (W. Zhang & Wirtz, 2017). An initial increase in biomass along with an increase in POC content is often observed until reaching a certain threshold. An excessively high POC content, particularly that found in coastal hypoxic zones, would then hinder the growth of macrobenthos and alter the community structure (Hyland et al., 2005; Pearson & Rosenberg, 1978). However, such a threshold might vary over a broad range depending on the configuration of the environment (e.g., lability of POC, level of toxic elements, oxygen) and community structure

of macrobenthos. Hyland et al. (2005) analyzed field data from 951 stations representing 7 coastal regions of the world and found that the threshold ranged between 1% and 3.5% in the POC content in sediment. The maximum POC content measured in the surface sediments of the ECS is approximately 1%, as shown in Figure 2c. This suggests that the threshold is not met in a major part of the study area, including the seasonal hypoxic zones and macrobenthos should not be affected by the degradation of POC in sediments. However, field surveys indicate a reduction in macrobenthos biomass in hypoxic zones compared to adjacent areas (Figure 5b), which seems to contradict the previous argument. One feasible explanation to reconcile this contradiction is that the reduction of macrobenthos biomass is mainly caused by exhaustion of oxygen in bottom water rather than degradation of POC in sediments. This implies that most oxygen is depleted in water with WOC as the major cause of hypoxia, which further supports the results of this study. Furthermore, anthropogenic impacts on coastal benthos, such as overfishing, pollution, habitat destruction and species invasions, introduce additional uncertainties to the modeling effort (Levin et al., 2009). The impact of intense trawling activities (S. Zhang et al., 2016) on the sedimentary system (Porz et al., 2021) also needs to be quantified. Future modeling work should explicitly include such human-induced disturbance to macrobenthos.

5. Conclusions

This study applied a coupled benthic-pelagic model to simulate ecosystem dynamics on the ECS shelf. Comparisons with field observations showed good performance of the model in reproducing the hydrographic and ecological environments, particularly for the hypoxic zone and SOC. Through an analysis of the model outputs for 6 yr, the following conclusions for spatiotemporal variations in the SOC and its relation to hypoxia are drawn.

On the ECS shelf, SOC is dominated either by porewater advective flux or bioturbation diffusive flux. Porewater advective DO flux is predominant in the TSS and RSA areas in summer, while the bioturbation diffusive DO flux is predominant in the CSD, ZMCMB and SWCIM areas. In the submerged river valley, both terms are low. The SOC in the TSS area is the highest in the entire study area. The SOC is higher at nearshore mud depocenters than at offshore mud depocenters. The temporal variation in the SOC shows a strong spatial heterogeneity. The SOC in the TSS area reaches a peak in winter and a trough in summer. Annual cycles with similar seasonality of the SOC exist at the CSD, ZMCMB and the submerged river valley. DO fluxes in these regions, as well as their synoptic variabilities, exhibit a peak in summer corresponding to primary production. The seasonal signal becomes weak on the middle and outer shelves.

The contribution of SOC to total local oxygen consumption was evaluated by comparing it to WOC below the pycnocline. Although the contribution of the summer SOC ranges between ~15% and ~80% in coastal waters, it is generally below ~40% in the hypoxic zone. The spatial distribution of SOC in summer is relatively steady from year to year, while the high WOC patches explain more about the interannual variation in the hypoxic zone. It is concluded that WOC is the major driver of the variation of hypoxia. It is worth noting that the variations within the benthic system in association with the hypoxic condition could be time- and site-specific due to complex pelagic-benthic coupling processes. In 2013, the less energetic hydrodynamics in the TSS area on the Changjiang bank aggravated both the WOC and the benthic bioturbation diffusive DO flux but substantially suppressed the porewater advective DO flux, which resulted in a net lower contribution of SOC to hypoxia. This mechanism for hypoxia north of 31°N on the Changjiang bank may shed light on other pelagic-benthic coupling processes in coastal shelf seas where hypoxia occurs on permeable sediments.

Data Availability Statement

The observational data employed in this study can be found in supplementary files. Model outputs for benthic oxygen flux can be accessed via the Science Data Bank, Chinese Academy of Sciences (CAS) repository with the DOI:10.11922/sciencedb.01234. The source code of TOCMAIM with a coupling interface to 3-D hydrodynamic biogeochemical models can be downloaded at http://dx.doi.org/10.17632/2vvny3xd85.2.

Acknowledgments
We thank two anonymous reviewers for their constructive comments. This study was jointly supported by the National Key Research & Development Program of China (Grant No. 2018YFD0900906), Leading Talents of Science and Technology Innovation in Zhejiang Provincial 10 Thousand Talents Program (Grant No. 2020R52038), the Natural Science Foundation of China (Grant No. 41876026), the Project of State Key Laboratory of Satellite Ocean Environment Dynamics (Grant Nos. SOEDZZ1905, SOEDZZ2001 and SOEDZZ2103), Scientific Research Fund of the Second Institute of Oceanography, MNR (Grant No. SL2102), Research Fund of Zhejiang Province (Grant No. 330000210130313013006) and National Programme on Global Change and Air-Sea Interaction (Phase II). It also contributes to the I2B project "Unravelling the linkages between benthic biological functioning, biogeochemistry and coastal morphodynamics—from big data to mechanistic modelling" funded by Helmholtz-Zentrum Hereon within the framework of the PoF IV program. The numerical simulations were performed in the high-performance computer "Mistral" at German Climate Computing Center (DKRZ) in Hamburg and the high-performance computer cluster system run by the computing and data sharing center of the State Key Laboratory of Satellite Ocean Environment Dynamics. We thank the Observation and Research Station of Yangtze River Delta Marine Ecosystems of Ministry of Natural Resources (http://yangtzeriverestuary.soed.org.cn/) for providing the observational data as well as all the crew members to conduct the surveys. This study is also part of the Long-Term Observation and Research Plan in the Changjiang Estuary and the Adjacent East China Sea (LORCE) program (Grant No. SZZ1601).

References

Atlas, R., Hoffman, R. N., Ardizzone, J., Leidner, S. M., Jusem, J. C., Smith, D. K., & Gombos, D. (2011). A cross-calibrated, multiplatform ocean surface wind velocity product for meteorological and oceanographic applications. *Bulletin of the American Meteorological Society*, *92*(2), 157–174. https://doi.org/10.1175/2010bams2946.1

Bleck, R. (2002). An oceanic general circulation model framed in hybrid isopycnic-Cartesian coordinates. *Ocean Modelling*, *4*(1), 55–88. https://doi.org/10.1016/S1463-5003(01)00012-9

Breitburg, D., Levin, L. A., Oschlies, A., Grégoire, M., Chavez, F. P., Conley, D. J., et al. (2018). Declining oxygen in the global ocean and coastal waters. *Science*, *359*(6371), eaam7240. https://doi.org/10.1126/science.aam7240

Briggs, K. B., Craig, J. K., Shivarudrappa, S., & Richards, T. M. (2017). Macrobenthos and megabenthos responses to long-term, large-scale hypoxia on the Louisiana continental shelf. *Marine Environmental Research*, *123*, 38–52. https://doi.org/10.1016/j.marenvres.2016.11.008

Cai, P., Shi, X., Moore, W. S., Peng, S., Wang, G., & Dai, M. (2014). 224Ra:228Th disequilibrium in coastal sediments: Implications for solute transfer across the sediment-water interface. *Geochimica et Cosmochimica Acta*, *125*, 68–84. https://doi.org/10.1016/j.gca.2013.09.029

Chai, F., Dugdale, R. C., Peng, T. H., Wilkerson, F. P., & Barber, R. T. (2002). One-dimensional ecosystem model of the equatorial Pacific upwelling system. Part I: Model development and silicon and nitrogen cycle. *Deep Sea Research Part II: Topical Studies in Oceanography*, *49*(13), 2713–2745. https://doi.org/10.1016/S0967-0645(02)00055-3

Chen, D. X. (Ed.). (1992). *Marine Atlas of Bohai Sea, Yellow Sea and East China Sea, Hydrology* (pp.13–96). China Ocean Press.

Chen, C.-C., Gong, G.-C., & Shiah, F.-K. (2007). Hypoxia in the East China Sea: One of the largest coastal low-oxygen areas in the world. *Marine Environmental Research*, *64*(4), 399–408. https://doi.org/10.1016/j.marenvres.2007.01.007

Chi, L., Song, X., Ding, Y., Yuan, Y., Wang, W., Cao, X., et al. (2021). Heterogeneity of the sediment oxygen demand and its contribution to the hypoxia off the Changjiang Estuary and its adjacent waters. *Marine Pollution Bulletin*, *172*, 112920. https://doi.org/10.1016/j.marpolbul.2021.112920

Chi, L., Song, X., Yuan, Y., Wang, W., Cao, X., Wu, Z., & Yu, Z. (2020). Main factors dominating the development, formation and dissipation of hypoxia off the Changjiang Estuary (CE) and its adjacent waters, China. *Environmental Pollution*, *265*, 115066. https://doi.org/10.1016/j.envpol.2020.115066

Conley, D. J., Paerl, H. W., Howarth, R. W., Boesch, D. F., Seitzinger, S. P., Havens, K. E., et al. (2009). Controlling eutrophication: Nitrogen and phosphorus. *Science*, *323*(5917), 1014–1015. https://doi.org/10.1126/science.1167755

Diaz, R. J., & Rosenberg, R. (2008). Spreading dead zones and consequences for marine ecosystems. *Science*, *321*(5891), 926–929. https://doi.org/10.1126/science.1156401

Egbert, G. D., & Erofeeva, S. Y. (2002). Efficient inverse modeling of barotropic ocean tides. *Journal of Atmospheric and Oceanic Technology*, *19*(2), 183–204. https://doi.org/10.1175/1520-0426(2002)019<0183:eimobo>2.0.co;2

Fennel, K., Gehlen, M., Brasseur, P., Brown, C. W., Ciavatta, S., Cossarini, G., et al. (2019). Advancing marine biogeochemical and ecosystem reanalyses and forecasts as tools for monitoring and managing ecosystem health. *Frontiers in Marine Science*, *6*(89). https://doi.org/10.3389/fmars.2019.00089

Fennel, K., Hu, J., Laurent, A., Marta-Almeida, M., & Hetland, R. (2013). Sensitivity of hypoxia predictions for the northern Gulf of Mexico to sediment oxygen consumption and model nesting. *Journal of Geophysical Research: Oceans*, *118*(2), 990–1002. https://doi.org/10.1002/jgrc.20077

Fennel, K., & Laurent, A. (2018). N and P as ultimate and proximate limiting nutrients in the northern Gulf of Mexico: Implications for hypoxia reduction strategies. *Biogeosciences*, *15*(10), 3121–3131. https://doi.org/10.5194/bg-15-3121-2018

Fennel, K., & Testa, J. M. (2019). Biogeochemical controls on coastal hypoxia. *Annual Review of Marine Science*, *11*(1), 105–130. https://doi.org/10.1146/annurev-marine-010318-095138

Fennel, K., Wilkin, J., Levin, J., Moisan, J., O'Reilly, J., & Haidvogel, D. (2006). Nitrogen cycling in the Middle Atlantic Bight: Results from a three-dimensional model and implications for the North Atlantic nitrogen budget. *Global Biogeochemical Cycles*, *20*(3), GB3007. https://doi.org/10.1029/2005GB002456

Ge, J., Shi, S., Liu, J., Xu, Y., Chen, C., Bellerby, R., & Ding, P. (2020). Interannual variabilities of nutrients and phytoplankton off the Changjiang Estuary in response to changing river inputs. *Journal of Geophysical Research: Oceans*, *125*(3), e2019JC015595. https://doi.org/10.1029/2019JC015595

Griffiths, J. R., Kadin, M., Nascimento, F. J. A., Tamelander, T., Törnroos, A., Bonaglia, S., et al. (2017). The importance of benthic-pelagic coupling for marine ecosystem functioning in a changing world. *Global Change Biology*, *23*(6), 2179–2196. https://doi.org/10.1111/gcb.13642

Große, F., Fennel, K., & Laurent, A. (2019). Quantifying the relative importance of riverine and open-ocean nitrogen sources for hypoxia formation in the northern Gulf of Mexico. *Journal of Geophysical Research: Oceans*, *124*(8), 5451–5467. https://doi.org/10.1029/2019JC015230

Haidvogel, D. B., Arango, H., Budgell, W. P., Cornuelle, B. D., Curchitser, E., Di Lorenzo, E., et al. (2008). Ocean forecasting in terrain-following coordinates: Formulation and skill assessment of the Regional Ocean Modeling System. *Journal of Computational Physics*, *227*(7), 3595–3624. https://doi.org/10.1016/j.jcp.2007.06.016

Halliwell, G. R. (1998). Simulation of North Atlantic decadal/multidecadal winter SST anomalies driven by basin-scale atmospheric circulation anomalies. *Journal of Physical Oceanography*, *28*(1), 5–21. https://doi.org/10.1175/1520-0485(1998)028<0005:sonadm>2.0.co;2

Hao, Q., Chai, F., Xiu, P., Bai, Y., Chen, J., Liu, C., et al. (2019). Spatial and temporal variation in chlorophyll a concentration in the Eastern China Seas based on a locally modified satellite dataset. *Estuarine, Coastal and Shelf Science*, *220*, 220–231. https://doi.org/10.1016/j.ecss.2019.01.004

Hersbach, H., Bell, B., Berrisford, P., Hirahara, S., Horányi, A., Muñoz-Sabater, J., et al. (2020). The ERA5 global reanalysis. *Quarterly Journal of the Royal Meteorological Society*, *146*(730), 1999–2049. https://doi.org/10.1002/qj.3803

Hetland, R. D., & DiMarco, S. F. (2008). How does the character of oxygen demand control the structure of hypoxia on the Texas-Louisiana continental shelf? *Journal of Marine Systems*, *70*(1), 49–62. https://doi.org/10.1016/j.jmarsys.2007.03.002

Hu, L., Shi, X., Yu, Z., Lin, T., Wang, H., Ma, D., et al. (2012). Distribution of sedimentary organic matter in estuarine-inner shelf regions of the East China Sea: Implications for hydrodynamic forces and anthropogenic impact. *Marine Chemistry*, *142–144*, 29–40. https://doi.org/10.1016/j.marchem.2012.08.004

Hyland, J., Balthis, L., Karakassis, I., Magni, P., Petrov, A., Shine, J., et al. (2005). Organic carbon content of sediments as an indicator of stress in the marine benthos. *Marine Ecology Progress Series*, *295*, 91–103. https://doi.org/10.3354/meps295091

Jia, J., Gao, J., Cai, T., Li, Y., Yang, Y., Wang, Y. P., et al. (2018). Sediment accumulation and retention of the Changjiang (Yangtze River) subaqueous delta and its distal muds over the last century. *Marine Geology*, *401*, 2–16. https://doi.org/10.1016/j.margeo.2018.04.005

Kelly, K. A., Thompson, L., Cheng, W., & Metzger, E. J. (2007). Evaluation of HYCOM in the Kuroshio Extension region using new metrics. *Journal of Geophysical Research*, *112*, C01004. https://doi.org/10.1029/2006JC003614

Kemp, W. M., Sampou, P. A., Garber, J., Tuttle, J., & Boynton, W. R. (1992). Seasonal depletion of oxygen from bottom waters of Chesapeake Bay: Roles of benthic and planktonic respiration and physical exchange processes. *Marine Ecology Progress Series*, *85*, 137–152. https://doi.org/10.3354/meps085137

Large, W. G., & Pond, S. (1981). Open ocean momentum flux measurements in moderate to strong winds. *Journal of Physical Oceanography*, *11*(3), 324–336. https://doi.org/10.1175/1520-0485(1981)011<0324:oomfmi>2.0.co;2

Laurent, A., Fennel, K., Cai, W.-J., Huang, W.-J., Barbero, L., & Wanninkhof, R. (2017). Eutrophication-induced acidification of coastal waters in the northern Gulf of Mexico: Insights into origin and processes from a coupled physical-biogeochemical model. *Geophysical Research Letters*, *44*(2), 946–956. https://doi.org/10.1002/2016GL071881

Levin, L. A., Ekau, W., Gooday, A. J., Jorissen, F., Middelburg, J. J., Naqvi, S. W. A., et al. (2009). Effects of natural and human-induced hypoxia on coastal benthos. *Biogeosciences*, *6*(10), 2063–2098. https://doi.org/10.5194/bg-6-2063-2009

Li, D., Zhang, J., Huang, D., Wu, Y., & Liang, J. (2002). Oxygen depletion off the Changjiang (Yangtze River) estuary. *Science in China—Series D: Earth Sciences*, *45*(12), 1137–1146. https://doi.org/10.1360/02yd9110

Liblik, T., Wu, Y., Fan, D., & Shang, D. (2020). Wind-driven stratification patterns and dissolved oxygen depletion off the Changjiang (Yangtze) Estuary. *Biogeosciences*, *17*(10), 2875–2895. https://doi.org/10.5194/bg-17-2875-2020

Liu, Z. X. (1997). Yangtze Shoal—A modern tidal sand sheet in the northwestern part of the East China Sea. *Marine Geology*, *137*(3), 321–330. https://doi.org/10.1016/S0025-3227(96)00026-6

Lu, X., Yu, H., Ying, M., Zhao, B., Zhang, S., Lin, L., et al. (2021). Western North Pacific tropical cyclone database created by the China Meteorological Administration. *Advances in Atmospheric Sciences*, *38*(4), 690–699. https://doi.org/10.1007/s00376-020-0211-7

Luo, Z., Zhu, J., Wu, H., & Li, X. (2017). Dynamics of the sediment plume over the Yangtze bank in the Yellow and East China seas. *Journal of Geophysical Research: Oceans*, *122*(12), 10073–10090. https://doi.org/10.1002/2017JC013215

Mears, C. A., Scott, J., Wentz, F. J., Ricciardulli, L., Leidner, S. M., Hoffman, R., & Atlas, R. (2019). A near-real-time version of the cross-calibrated multiplatform (CCMP) ocean surface wind velocity data Set. *Journal of Geophysical Research: Oceans*, *124*(10), 6997–7010. https://doi.org/10.1029/2019JC015367

Meile, C., & Van Cappellen, P. (2005). Particle age distributions and O2 exposure times: Timescales in bioturbated sediments. *Global Biogeochemical Cycles*, *19*, GB3013. https://doi.org/10.1029/2004GB002371

Meng, Q., Xuan, J., Zhang, W., Zhou, F., Hao, Q., Zhao, Q., & Schrum, C. (2020). Impact of submesoscale vertical advection on primary productivity in the southern East China Sea. *Journal of Geophysical Research: Biogeosciences*, *125*, e2019JG005540. https://doi.org/10.1029/2019JG005540

Meysman, F. J. R., Middelburg, J. J., & Heip, C. H. R. (2006). Bioturbation: A fresh look at Darwin's last idea. *Trends in Ecology & Evolution*, *21*(12), 688–695. https://doi.org/10.1016/j.tree.2006.08.002

Middelburg, J. J. (2018). Reviews and syntheses: To the bottom of carbon processing at the seafloor. *Biogeosciences*, *15*(2), 413–427. https://doi.org/10.5194/bg-15-413-2018

Ni, X., Huang, D., Zeng, D., Zhang, T., Li, H., & Chen, J. (2016). The impact of wind mixing on the variation of bottom dissolved oxygen off the Changjiang Estuary during summer. *Journal of Marine Systems*, *154*, 122–130. https://doi.org/10.1016/j.jmarsys.2014.11.010

Pearson, T. H., & Rosenberg, R. (1978). Macrobenthic succession in relation to organic enrichment and pollution of the marine environment. *Oceanography and Marine Biology an Annual Review*, *16*, 229–311. https://doi.org/10.2983/035.034.0121u1.10

Porz, L., Zhang, W., Hanebuth, T. J. J., & Schrum, C. (2021). Physical processes controlling mud depocenter development on continental shelves—Geological, oceanographic, and modeling concepts. *Marine Geology*, *432*, 106402. https://doi.org/10.1016/j.margeo.2020.106402

Rabalais, N. N., Díaz, R. J., Levin, L. A., Turner, R. E., Gilbert, D., & Zhang, J. (2010). Dynamics and distribution of natural and human-caused hypoxia. *Biogeosciences*, *7*(2), 585–619. https://doi.org/10.5194/bg-7-585-2010

Rabouille, C., Conley, D. J., Dai, M. H., Cai, W. J., Chen, C. T. A., Lansard, B., et al. (2008). Comparison of hypoxia among four river-dominated ocean margins: The Changjiang (Yangtze), Mississippi, Pearl, and Rhône rivers. *Continental Shelf Research*, *28*(12), 1527–1537. https://doi.org/10.1016/j.csr.2008.01.020

Redfield, A. C. (1934). On the proportions of organic derivatives in sea water and their relation to the composition of plankton. In *James Johnstone memorial volume* (pp. 176–192). Liverpool: University Press of Liverpool.

Reynolds, R. W., Smith, T. M., Liu, C., Chelton, D. B., Casey, K. S., & Schlax, M. G. (2007). Daily high-resolution-blended analyses for sea surface temperature. *Journal of Climate*, *20*(22), 5473–5496. https://doi.org/10.1175/2007jcli1824.1

Santos, I. R., Eyre, B. D., & Huettel, M. (2012). The driving forces of porewater and groundwater flow in permeable coastal sediments: A review. *Estuarine, Coastal and Shelf Science*, *98*, 1–15. https://doi.org/10.1016/j.ecss.2011.10.024

Sasaki, H., Klein, P., Qiu, B., & Sasai, Y. (2014). Impact of oceanic-scale interactions on the seasonal modulation of ocean dynamics by the atmosphere. *Nature Communication*, *5*, 5636. https://doi.org/10.1038/ncomms6636

Shchepetkin, A. F., & McWilliams, J. C. (2005). The regional oceanic modeling system (ROMS): A split-explicit, free-surface, topography-following-coordinate oceanic model. *Ocean Modelling*, *9*(4), 347–404. https://doi.org/10.1016/j.ocemod.2004.08.002

Snelgrove, P. V. R., Soetaert, K., Solan, M., Thrush, S., Wei, C.-L., Danovaro, R., et al. (2018). Global carbon cycling on a heterogeneous seafloor. *Trends in Ecology & Evolution*, *33*(2), 96–105. https://doi.org/10.1016/j.tree.2017.11.004

Song, G., Liu, S., Zhu, Z., Zhai, W., Zhu, C., & Zhang, J. (2016). Sediment oxygen consumption and benthic organic carbon mineralization on the continental shelves of the East China Sea and the Yellow Sea. *Deep Sea Research Part II: Topical Studies in Oceanography*, *124*, 53–63. https://doi.org/10.1016/j.dsr2.2015.04.012

Testa, J. M., Clark, J. B., Dennison, W. C., Donovan, E. C., Fisher, A. W., Ni, W., et al. (2017). Ecological forecasting and the science of hypoxia in Chesapeake Bay. *BioScience*, *67*(7), 614–626. https://doi.org/10.1093/biosci/bix048

Vaquer-Sunyer, R., & Duarte, C. M. (2008). Thresholds of hypoxia for marine biodiversity. *Proceedings of the National Academy of Sciences*, *105*(40), 15452–15457. https://doi.org/10.1073/pnas.0803833105

Wang, B., Chen, J., Jin, H., Li, H., Huang, D., & Cai, W.-J. (2017). Diatom bloom–derived bottom water hypoxia off the Changjiang estuary, with and without typhoon influence. *Limnology & Oceanography*, *62*(4), 1552–1569. https://doi.org/10.1002/lno.10517

Wang, B., Wei, Q., Chen, J., & Xie, L. (2012). Annual cycle of hypoxia off the Changjiang (Yangtze River) Estuary. *Marine Environmental Research*, *77*, 1–5. https://doi.org/10.1016/j.marenvres.2011.12.007

Wang, C., Hao, Z., Gao, J., Feng, Z., Ding, Y., Zhang, C., & Zou, X. (2020). Reservoir construction has reduced organic carbon deposition in the East China Sea by half since 2006. *Geophysical Research Letters*, *47*(17), e2020GL087357. https://doi.org/10.1029/2020GL087357

Wang, H., Dai, M., Liu, J., Kao, S.-J., Zhang, C., Cai, W.-J., et al. (2016). Eutrophication–driven hypoxia in the East China Sea off the Changjiang Estuary. *Environmental Science & Technology*, *50*(5), 2255–2263. https://doi.org/10.1021/acs.est.5b06211

Wang, K., Cai, W.-J., Chen, J., Kirchman, D., Wang, B., Fan, W., & Huang, D. (2021). Climate and human-driven variability of summer hypoxia on a large river-dominated shelf as revealed by a hypoxia index. *Frontiers in Marine Science*, *8*, 634184. https://doi.org/10.3389/fmars.2021.634184

Wang, K., Chen, J., Jin, H., Li, H., Gao, S., Xu, J., et al. (2014). Summer nutrient dynamics and biological carbon uptake rate in the Changjiang River plume inferred using a three end-member mixing model. *Continental Shelf Research*, *91*, 192–200. https://doi.org/10.1016/j.csr.2014.09.013

Wang, Y., Wu, H., Gao, L., Shen, F., & Liang, X. S. (2019). Spatial distribution and physical controls of the spring algal blooming off the Changjiang River estuary. *Estuaries and Coasts*, *42*(4), 1066–1083. https://doi.org/10.1007/s12237-019-00545-x

Wei, L., Cai, P., Shi, X., Cai, W., Liu, W., Hong, Q., et al. (2021). Winter mixing accelerates decomposition of sedimentary organic carbon in seasonally hypoxic coastal seas. *Geochimica et Cosmochimica Acta*. https://doi.org/10.1016/j.gca.2021.11.003

Wei, H., He, Y., Li, Q., Liu, Z., & Wang, H. (2007). Summer hypoxia adjacent to the Changjiang Estuary. *Journal of Marine Systems*, *67*(3), 292–303. https://doi.org/10.1016/j.jmarsys.2006.04.014

Wentz, F. J. J., Scott, J., Hoffman, R., Leidner, M., Atlas, R., & Ardizzone, J. (2015). *Remote sensing systems cross-calibrated multi-platform (CCMP) 6-hourly ocean vector wind analysis product on 0.25 deg grid, Version 2.0*. Remote Sensing Systems. Retrieved from www.remss.com/measurements/ccmp

Wu, R. S. S. (2002). Hypoxia: From molecular responses to ecosystem responses. *Marine Pollution Bulletin*, *45*(1), 35–45. https://doi.org/10.1016/S0025-326X(02)00061-9

Xiu, P., & Chai, F. (2014). Connections between physical, optical and biogeochemical processes in the Pacific Ocean. *Progress in Oceanography*, *122*, 30–53. https://doi.org/10.1016/j.pocean.2013.11.008

Xuan, J., Yang, Z., Huang, D., Wang, T., & Zhou, F. (2016). Tidal residual current and its role in the mean flow on the Changjiang Bank. *Journal of Marine Systems*, *154*, 66–81. https://doi.org/10.1016/j.jmarsys.2015.04.005

Yan, Y., Chai, F., Xue, H., & Wang, G. (2020). Record-breaking sea surface temperatures in the Yellow and East China seas. *Journal of Geophysical Research: Oceans*, *125*(8). e2019JC015883. https://doi.org/10.1029/2019JC015883

Ying, M., Zhang, W., Yu, H., Lu, X., Feng, J., Fan, Y., et al. (2014). An overview of the China Meteorological Administration tropical cyclone database. *Journal of Atmospheric and Oceanic Technology*, *31*(2), 287–301. https://doi.org/10.1175/jtech-d-12-00119.1

Yu, L., Fennel, K., Laurent, A., Murrell, M. C., & Lehrter, J. C. (2015). Numerical analysis of the primary processes controlling oxygen dynamics on the Louisiana shelf. *Biogeosciences*, *12*(7), 2063–2076. https://doi.org/10.5194/bg-12-2063-2015

Yu, P., Xue, B., Pan, J., Zheng, M., & Zhang, H. (2011). Impact of sediment grain size on the distribution of organic matter in Changjiang River Estuary and East China Sea (in Chinese with English abstract). *Journal of Marine Sciences*, *29*(003), 202–208. https://doi.org/10.3969/j.issn.1001-909X.2011.03.024

Zhang, H., Fennel, K., Laurent, A., & Bian, C. (2020). A numerical model study of the main factors contributing to hypoxia and its interannual and short-term variability in the East China Sea. *Biogeosciences*, *17*(22), 5745–5761. https://doi.org/10.5194/bg-17-5745-2020

Zhang, H., & Li, S. (2010). Effects of physical and biochemical processes on the dissolved oxygen budget for the Pearl River Estuary during summer. *Journal of Marine Systems*, *79*(1), 65–88. https://doi.org/10.1016/j.jmarsys.2009.07.002

Zhang, H., Zhao, L., Sun, Y., Wang, J., & Wei, H. (2017). Contribution of sediment oxygen demand to hypoxia development off the Changjiang Estuary. *Estuarine, Coastal and Shelf Science*, *192*, 149–157. https://doi.org/10.1016/j.ecss.2017.05.006

Zhang, S., Jin, S., Zhang, H., Fan, W., Tang, F., & Yang, S. (2016). Distribution of bottom trawling effort in the Yellow Sea and East China Sea. *PLoS One*, *11*(11), e0166640. https://doi.org/10.1371/journal.pone.0166640

Zhang, W., Jin, H., Yao, X., Ji, Z., Zhang, X., Yu, X., et al. (2015). Grain size composition and transport of sedimentary organic carbon in the Changjiang River (Yangtze River) Estuary and Hangzhou Bay and their adjacent waters. *Acta Oceanologica Sinica*, *34*(10), 46–56. https://doi.org/10.1007/s13131-015-0711-y

Zhang, W., Neumann, A., Daewel, U., Wirtz, K., van Beusekom, J. E. E., Eisele, A., et al. (2021). Quantifying importance of macrobenthos for benthic-pelagic coupling in a temperate coastal shelf sea. *Journal of Geophysical Research: Oceans*, *126*. e2020JC016995. https://doi.org/10.1029/2020JC016995

Zhang, W., & Wirtz, K. (2017). Mutual dependence between sedimentary organic carbon and infaunal macrobenthos resolved by mechanistic modeling. *Journal of Geophysical Research: Biogeosciences*, *122*(10), 2509–2526. https://doi.org/10.1002/2017JG003909

Zhang, W., Wirtz, K., Daewel, U., Wrede, A., Kröncke, I., Kuhn, G., et al. (2019). The budget of macrobenthic reworked organic carbon: A modeling case study of the north sea. *Journal of Geophysical Research: Biogeosciences*, *124*(6), 1446–1471. https://doi.org/10.1029/2019JG005109

Zhang, W., Wu, H., Hetland, R. D., & Zhu, Z. (2019). On mechanisms controlling the seasonal hypoxia hot spots off the Changjiang River estuary. *Journal of Geophysical Research: Oceans*, *124*(12), 8683–8700. https://doi.org/10.1029/2019JC015322

Zhang, W., Wu, H., & Zhu, Z. (2018). Transient hypoxia extent off Changjiang River estuary due to mobile Changjiang River plume. *Journal of Geophysical Research: Oceans*, *123*(12), 9196–9211. https://doi.org/10.1029/2018JC014596

Zhao, B., Yao, P., Bianchi, T. S., Arellano, A. R., Wang, X., Yang, J., et al. (2018). The remineralization of sedimentary organic carbon in different sedimentary regimes of the Yellow and East China Seas. *Chemical Geology*, *495*, 104–117. https://doi.org/10.1016/j.chemgeo.2018.08.012

Zhou, F., Chai, F., Huang, D., Wells, M., Ma, X., Meng, Q., et al. (2020). Coupling and decoupling of high biomass phytoplankton production and hypoxia in a highly dynamic coastal system: The Changjiang (Yangtze River) estuary. *Frontiers in Marine Science*, *7*, 259. https://doi.org/10.3389/fmars.2020.00259

Zhou, F., Chai, F., Huang, D., Xue, H., Chen, J., Xiu, P., et al. (2017). Investigation of hypoxia off the Changjiang Estuary using a coupled model of ROMS-CoSiNE. *Progress in Oceanography*, *159*, 237–254. https://doi.org/10.1016/j.pocean.2017.10.008

Zhou, F., Huang, D., Ni, X., Xuan, J., Zhang, J., & Zhu, K. (2010). Hydrographic analysis on the multi-time scale variability of hypoxia adjacent to the Changjiang River Estuary. *Acta Ecologica Sinica*, *30*(17), 4728–4740.

Zhou, F., Xue, H., Huang, D., Xuan, J., Ni, X., Xiu, P., & Hao, Q. (2015). Cross-shelf exchange in the shelf of the East China Sea. *Journal of Geophysical Research: Oceans*, *120*(3), 1545–1572. https://doi.org/10.1002/2014JC010567

Zhou, J., Zhu, Z.-Y., Hu, H.-T., Zhang, G.-L., & Wang, Q.-Q. (2021). Clarifying water column respiration and sedimentary oxygen respiration under oxygen depletion off the Changjiang Estuary and Adjacent East China sea. *Frontiers in Marine Science*, *7*, 623581. https://doi.org/10.3389/fmars.2020.623581

Zhu, Z.-Y., Hu, J., Song, G.-D., Wu, Y., Zhang, J., & Liu, S.-M. (2016). Phytoplankton-driven dark plankton respiration in the hypoxic zone off the Changjiang Estuary, revealed by in vitro incubations. *Journal of Marine Systems*, *154*, 50–56. https://doi.org/10.1016/j.jmarsys.2015.04.009

Zhu, Z.-Y., Zhang, J., Wu, Y., Zhang, Y.-Y., Lin, J., & Liu, S.-M. (2011). Hypoxia off the Changjiang (Yangtze River) estuary: Oxygen depletion and organic matter decomposition. *Marine Chemistry*, *125*(1), 108–116. https://doi.org/10.1016/j.marchem.2011.03.005